Received: 7 September 2018 | Accepted: 26 January 2019

DOI: 10.1111/gcb.14604

PRIMARY RESEARCH ARTICLE

WILEY Global Change Biology

# Effects of mesophyll conductance on vegetation responses to elevated $CO_2$ concentrations in a land surface model

Jürgen Knauer[1,2] | Sönke Zaehle[1,3] | Martin G. De Kauwe[4] | Nur H. A. Bahar[5] | John R. Evans[6] | Belinda E. Medlyn[7] | Markus Reichstein[1,3] | Christiane Werner[8]

[1]Department of Biogeochemical Integration, Max Planck Institute for Biogeochemistry, Jena, Germany

[2]International Max Planck Research School for Global Biogeochemical Cycles (IMPRS gBGC), Jena, Germany

[3]Michael-Stifel Center Jena for Data-Driven and Simulation Science, Jena, Germany

[4]ARC Centre of Excellence for Climate Extremes and the Climate Change Research Centre, University of New South Wales, Sydney, NSW, Australia

[5]ARC Centre of Excellence in Plant Energy Biology, Division of Plant Sciences, Research School of Biology, Australian National University, Canberra, ACT, Australia

[6]ARC Centre of Excellence for Translational Photosynthesis, Division of Plant Sciences, Research School of Biology, Australian National University, Canberra, ACT, Australia

[7]Hawkesbury Institute for the Environment, Western Sydney University, Richmond, NSW, Australia

[8]Department of Ecosystem Physiology, University of Freiburg, Freiburg, Germany

**Correspondence**
Jürgen Knauer, Department of Biogeochemical Integration, Max Planck Institute for Biogeochemistry, Jena, Germany.
Email: jknauer@bgc-jena.mpg.de

**Funding information**
H2020 European Research Council, Grant/Award Number: 647204; Australian Research Council, Grant/Award Number: CE170100023

## Abstract

Mesophyll conductance ($g_m$) is known to affect plant photosynthesis. However, $g_m$ is rarely explicitly considered in land surface models (LSMs), with the consequence that its role in ecosystem and large-scale carbon and water fluxes is poorly understood. In particular, the different magnitudes of $g_m$ across plant functional types (PFTs) are expected to cause spatially divergent vegetation responses to elevated $CO_2$ concentrations. Here, an extensive literature compilation of $g_m$ across major vegetation types is used to parameterize an empirical model of $g_m$ in the LSM JSBACH and to adjust photosynthetic parameters based on simulated $A_n - C_i$ curves. We demonstrate that an explicit representation of $g_m$ changes the response of photosynthesis to environmental factors, which cannot be entirely compensated by adjusting photosynthetic parameters. These altered responses lead to changes in the photosynthetic sensitivity to atmospheric $CO_2$ concentrations which depend both on the magnitude of $g_m$ and the climatic conditions, particularly temperature. We then conducted simulations under ambient and elevated (ambient + 200 μmol/mol) $CO_2$ concentrations for contrasting ecosystems and for historical and anticipated future climate conditions (representative concentration pathways; RCPs) globally. The $g_m$-explicit simulations using the RCP8.5 scenario resulted in significantly higher increases in gross primary productivity (GPP) in high latitudes (+10% to + 25%),, intermediate increases in temperate regions (+5% to 15%), and slightly lower to moderately higher responses in tropical regions (−2% to +5%), which summed up to moderate GPP increases globally. Similar patterns were found for transpiration, but with a lower magnitude. Our results suggest that the effect of an explicit representation of $g_m$ is most important for simulated carbon and water fluxes in the boreal zone, where a cold climate coincides with evergreen vegetation.

**KEYWORDS**
elevated $CO_2$ concentrations, land surface modeling, mesophyll conductance, photosynthetic $CO_2$ sensitivity, representative concentration pathways

## 1 | INTRODUCTION

The representation of photosynthesis in land surface models (LSMs) is critical for simulating the response of the terrestrial biosphere to global environmental change (Booth et al., 2012; Rogers et al., 2017), the land uptake of $CO_2$, as well as the coupling of the water and carbon cycles. The photosynthesis schemes embedded within state-of-the-art LSMs commonly assume that the $CO_2$ concentration available for carboxylation equals the $CO_2$ concentration in the sub-stomatal cavity, that is the intercellular $CO_2$ concentration ($C_i$). This corresponds to the assumption that the conductance to $CO_2$ transfer within the leaf (mesophyll conductance, $g_m$) is infinite, and that the $CO_2$ concentration at the actual place of carboxylation in the chloroplast stroma (chloroplastic $CO_2$ concentration, $C_c$) equals $C_i$. However, evidence has clearly shown that $g_m$ is finite (Flexas, Ribas-Carbó, Diaz-Espejo, Galmés, & Medrano, 2008; Warren, 2008) and that it causes a clear drawdown of the $CO_2$ concentration between the sub-stomatal cavity and the chloroplast stroma. The magnitude of this drawdown depends both on $g_m$ and the photosynthetic capacity of the leaf, which is reflected in the definition of $g_m$: $g_m = A_n/(C_i - C_c)$, where $A_n$ is net assimilation. Replacing $C_i$ with $C_c$ as the available $CO_2$ concentration for photosynthesis has been shown to change the response of simulated photosynthesis to environmental drivers (Niinemets, Díaz-Espejo, Flexas, Galmés, & Warren, 2009), which has important implications for large-scale simulations of land carbon uptake (Sun, Gu, Dickinson, Norby et al., 2014).

$g_m$ is a complex physiological property which integrates several leaf-internal sub-conductances in both the gaseous and liquid phase, including the intercellular airspace, cell walls, plasma membranes, cytoplasm, and the chloroplast envelopes and stroma (Evans, Kaldenhoff, Genty, & Terashima, 2009). $g_m$ is known to change dynamically in response to several environmental stimuli at the time scale of minutes (Warren, 2008). At the same time, its absolute magnitude is constrained by leaf anatomical and structural traits (e.g. cell wall thickness, chloroplast surface area attached to the intercellular airspaces (Tomás et al., 2013)), with the consequence that the values of $g_m$ differ considerably among vegetation types (Flexas et al., 2008).

Despite its important role in photosynthesis and the distinct differences across plant functional types (PFTs), $g_m$ is at present not explicitly considered in the vast majority of LSMs for two main reasons: (1) the current process understanding of $g_m$ is severely limited (Rogers et al., 2017) as its response to environmental drivers, foremost light and $CO_2$ concentration but also temperature, is largely unknown and currently an area of intensive research (von Caemmerer & Evans, 2015; Gu & Sun, 2014; Tazoe, Caemmerer, Badger, & Evans, 2009; Théroux-Rancourt & Gilbert, 2017; Xiong et al., 2015), and (2) the effects of $g_m$ are implicitly included in current models since the overestimation of $CO_2$ available for photosynthesis is compensated for by an underestimated (apparent) photosynthetic capacity. This means that parameters representing photosynthetic capacity, which are currently estimated on a $C_i$-basis, would need to be re-estimated on a $C_c$-basis if $g_m$ were to be explicitly considered in models (Sun, Gu, Dickinson, Pallardy et al., 2014).

It is likely for these two complications that so far only one study (Sun, Gu, Dickinson, Norby et al., 2014) focused on the effects of an explicit representation of $g_m$ in a LSM (the Community Land Model 4.5). Sun, Gu, Dickinson, Norby et al. (2014) showed that the overestimation of the available $CO_2$ concentration for photosynthesis due to the assumption of an infinite $g_m$ leads to an underestimation of the photosynthetic sensitivity to rising atmospheric $CO_2$ concentrations ($C_a$). As a consequence, replacing the implicit simulation of $g_m$ with an explicit one significantly increased the responsiveness of GPP (+16% from 1901 to 2010) to rising $C_a$ as long as $C_a$ was not saturating.

The stronger response of photosynthesis to rising atmospheric $CO_2$ concentrations with an explicitly modeled $g_m$ as shown in the study by Sun, Gu, Dickinson, Norby et al. (2014) implies that the physiological responses to rising atmospheric $CO_2$ concentrations will vary among plant groups that have intrinsically different values of $g_m$. Consequently, it might be hypothesized that photosynthesis of plants with a low $g_m$ (e.g. evergreen species) are more responsive to rising atmospheric $CO_2$ concentrations than plants with a higher $g_m$ (e.g. herbaceous plants), which potentially gives the former plant group a relative advantage over the latter in a high $CO_2$ world (Niinemets, Flexas, & Peñuelas, 2011). A stronger response of photosynthesis to $C_a$ is likely to also affect stomatal conductance ($g_s$) given that $g_s$ and $A_n$ are tightly coupled (Wong, Cowan, & Farquhar, 1979). As a consequence, the consideration of $g_m$ is expected to have important implications for both terrestrial carbon and water fluxes, as well as their coupling (e.g. water-use efficiency, Flexas et al., 2016). Such plant type-specific physiological responses would thus not only have important implications for the future global distribution of vegetation types, but also for large-scale patterns of biogeochemical cycles and associated physical climate feedbacks (e.g. evaporative cooling).

In this paper, we explore whether $g_m$ has implications for simulations of future global carbon and water fluxes, and to what extent the effects are expected to differ among vegetation types and climatic conditions. In the following, we (1) compile a global database of $g_m$ measurements, (2) describe the $g_m$ model and its incorporation into the LSM JSBACH (Knauer, Werner, & Zaehle, 2015; Reick, Raddatz, Brovkin, & Gayler, 2013), (3) outline the model parameterization and the necessary adjustment of photosynthetic parameters, (4) analyze the effects of an explicit $g_m$ on the photosynthetic sensitivity to $C_a$ at the leaf- and ecosystem level, and (5) investigate its relevance for future carbon and water fluxes globally.

## 2 | METHODS

To investigate the effects of $g_m$ on simulations of water and carbon fluxes, we tested two different approaches in the LSM JSBACH:

> **Implicit $g_m$:** Effects of $g_m$ are considered implicitly by employing apparent ($C_i$-based) photosynthetic parameters. This represents the current scenario in most LSMs.

**TABLE 1** Environmental responses considered in the $g_m$ model versions implemented in this study

| Model version | Temperature | Soil moisture | Canopy profile | Intercellular $CO_2$ concentration | Light |
|---|---|---|---|---|---|
| *Exp* | x | x | x | | |
| *ExpC* | x | x | x | x | |
| *ExpL* | x | x | x | | x |
| *ExpCL* | x | x | x | x | x |

Rubisco kinetic parameters were taken from Bernacchi et al. (2001). This model version is denoted as ***Imp***.

**Explicit $g_m$**: $g_m$ is modeled explicitly as described in Section 2.1. Rubisco kinetic parameters were taken from Bernacchi et al. (2002), and were determined on a $C_c$-basis. Four sub-versions (denoted as ***Exp***, ***ExpC***, ***ExpL***, ***ExpCL***) were implemented, which differ with respect to whether $g_m$ is affected by $C_i$ and/or light (Table 1). The effect of these two factors is contentious in the literature (Gu & Sun, 2014; Théroux-Rancourt & Gilbert, 2017), hence it is relevant to investigate their potential sensitivities to simulations of photosynthesis at the leaf to the global scale.

Note that the two approaches differ only in the consideration of $g_m$ (included implicitly or explicitly) and the Rubisco kinetic parameters (Michaelis-Menten constants for $CO_2$ ($K_c$) and $O_2$ ($K_o$), photorespiratory $CO_2$ compensation point ($\Gamma^*$)) as well as their temperature responses (see Appendix S1 for model formulations and Table S1 for parameter values).

## 2.1 | Mesophyll conductance model

The $g_m$ model implemented here is a multiplicative formulation, in which a PFT-specific maximum (i.e. unstressed) value of $g_m$ at the reference temperature of 25°C ($g_{m,max25}$) is modified by environmental factors:

$$g_m = \max(g_{m,min}, g_{m,max25} f_1(N) f_2(T_l) f_3(\theta) f_4(C_i) f_5(Q_a)) \quad (1)$$

where N is leaf nitrogen content, $T_l$ is leaf temperature, $\theta$ is soil moisture content, $C_i$ is intercellular $CO_2$ concentration, $Q_a$ is absorbed photosynthetic photon flux density, and $f$ denotes "function of". $g_{m,min}$ is defined as $g_{m,min} = f_{min} \times g_{m,max25}$, and accounts for the fact that $g_m$ does not decrease to zero even under unfavorable conditions such as severe water stress (e.g. Galmés, Medrano, & Flexas, 2007). $f_{min}$ was parameterized from data presented in Delfine, Loreto, Pinelli, Tognetti, and Alvino (2005), Galmés, Abadía, Medrano, and Flexas (2007), and Galmés, Medrano et al. (2007) as $f_{min} = 0.15$. In Equation (1), $g_{m,max25}$ and $f_1$ represent leaf structural determinants of $g_m$, whereas $f_2 - f_5$ describe instantaneous physiological responses. Note that the last two terms in Equation (1) ($f_4$ and $f_5$) are only considered in some model versions (Table 1). Acclimation of $g_m$ to elevated $CO_2$ was not considered in the model as measured $g_m$ of plants grown under ambient and elevated $CO_2$ concentrations did not show consistent differences (Kitao et al., 2015; Mizokami, Noguchi, Kojima, Sakakibara, & Terashima, 2018; Singsaas, Ort, & Delucia, 2003).

### 2.1.1 | Canopy profile

$g_m$ generally declines with depth through the canopy, and is usually higher in sun than in shade leaves (Hanba, Kogami, & Terashima, 2002; Piel, Frak, Roux, & Genty, 2002). It has been found that $g_m$ varies in a similar manner to photosynthetic capacity (or N) across the canopy profile (Montpied, Granier, & Dreyer, 2009). This decline with canopy depth might be related to the relatively low mesophyll thickness and the lower chloroplast surface area exposed to the intercellular airspaces in shade-adapted leaves (Evans, Caemmerer, Setchell, & Hudson, 1994; Hanba et al., 2002). Here, we implemented the following canopy profile of $g_m$:

$$f_1(N) = e^{-k_n L} \quad (2)$$

where $k_n$ is the canopy nitrogen extinction coefficient and $L$ is the leaf area index (LAI). $k_n$ was assumed to be 0.11 following Zaehle and Friend (2010). Thus, the canopy gradient of $g_m$ equals the one of $V_{cmax}$ and $J_{max}$ in the model. Such a behavior was confirmed by several studies (Han, Iio, Naramoto, & Kakubari, 2010; Montpied et al., 2009; Warren, Löw, Matyssek, & Tausz, 2007), but also higher (Zhang & Yin, 2012) and lower (Cano et al., 2011; Niinemets, Cescatti, Rodeghiero, & Tosens, 2006) gradients for $g_m$ compared to $V_{cmax}$ have been found, suggesting that $k_n$ is site- and probably PFT-specific (Warren et al., 2007).

### 2.1.2 | Temperature response

The temperature response of $g_m$ is the result of different physical and physiological processes in mesophyll cells (e.g. solubility and diffusivity of $CO_2$ in water), and the response is likely to differ across cell compartments, for example, membranes and cell walls (Evans & von Caemmerer, 2013). The overall response of $g_m$ to leaf temperature can be described by a modified Arrhenius function (Johnson, Eyring, & Williams, 1942):

$$f_2(T_l) = \exp\left(\frac{H_a(T_l - T_{ref})}{T_{ref} R T_l}\right) \frac{1 + \exp\left(\frac{T_{ref}\Delta S - H_d}{T_{ref} R}\right)}{1 + \exp\left(\frac{T_l \Delta S - H_d}{T_l R}\right)} \quad (3)$$

where $H_a$ is the activation energy (J/mol), $H_d$ is the deactivation energy (J/mol), $\Delta S$ is the entropy term (J $mol^{-1}$ $K^{-1}$) (see Table S1 for parameter values), $T_l$ is the leaf temperature (K), $T_{ref}$ is the reference temperature (298.15 K), and $R$ is the universal gas constant (8.314 J $mol^{-1}$

$K^{-1}$). Equation (3) was parameterized according to Bernacchi, Portis, Nakano, Caemmerer, and Long (2002) and shows a temperature optimum close to 35.5°C. The use of the parameter values reported in Bernacchi et al. (2002) is consistent with the $C_c$-based Rubisco kinetic parameters used in this study ($K_{o,Cc}$, $K_{c,Cc}$, $\Gamma^*_{Cc}$, Appendix S1), which were derived assuming the same temperature response of $g_m$ (Equation (3)). Published temperature responses of $g_m$ differ with respect to the behavior at high temperatures, and both hump-shaped (Egea, González-Real, Baille, Nortes, & Diaz-Espejo, 2011), as well as monotonously increasing responses (Scafaro, Caemmerer, Evans, & Atwell, 2011) have been documented. Similarly, $H_a$ is likely to be species-specific (Walker, Ariza, Kaines, Badger, & Cousins, 2013), though no clear patterns across species and growth conditions have been identified (von Caemmerer & Evans, 2015). Thus, parameters in Equation (3) were assumed to be identical for all vegetation types.

### 2.1.3 | Soil moisture response

The decline of $g_m$ with increasing soil water stress has been widely reported (e.g. Galmés, Medrano et al., 2007; Misson, Limousin, Rodriguez, & Letts, 2010; Varone et al., 2012), and has been attributed to the role of aquaporins in leaf-internal $CO_2$ transport (Miyazawa, Yoshimura, Shinzaki, Maeshima, & Miyake, 2008; Perez-Martin et al., 2014). Here, we implemented the following soil moisture dependence of $g_m$:

$$f_3(\theta) = \begin{cases} 1 & \theta \geq \theta_{crit} \\ \left[\frac{\theta-\theta_{wilt}}{\theta_{crit}-\theta_{wilt}}\right]^{q_m} & \theta < \theta_{crit} \\ 0 & \theta \leq \theta_{wilt} \end{cases} \quad (4)$$

where $\theta$ is soil moisture (m), $\theta_{wilt}$ is the permanent wilting point (m), below which water stress is at its maximum, and $\theta_{crit}$ is the critical soil moisture content (m), which marks the onset of soil water stress. $\theta_{wilt}$ and $\theta_{crit}$ are constant fractions (0.32 and 0.7 for $\theta_{wilt}$ and $\theta_{crit}$, respectively) of the field capacity, which is calculated depending on the grain size distribution of the soil. Equation (4) is applied to $g_m$, $g_s$, and leaf biochemistry ($V_{cmax}$ and $J_{max}$) but with different sensitivities (i.e. different values of the exponent $q$, i.e. $q_m$, $q_s$, and $q_b$ for $g_m$, $g_s$, and leaf biochemistry, respectively). Using the same formulation, Egea, Verhoef, and Vidale (2011) found that imposing the highest sensitivity to $g_m$, then to $g_s$, and finally to $V_{cmax}$ and $J_{max}$ best captured the behavior of photosynthesis under water stressed conditions for a variety of species from different PFTs. The $q$ parameters were defined accordingly as $q_m$ = 0.75, $q_s$ = 0.50, and $q_b$ = 0.25 for all PFTs.

### 2.1.4 | Response to intercellular $CO_2$ concentration

Most studies investigating the response of $g_m$ to $C_i$ have found a continuous decrease of $g_m$ with increasing $C_i$ under field conditions (i.e. $C_i$ above c. 200 μmol/mol) (Flexas et al., 2007; Hassiotou, Ludwig, Renton, Veneklaas, & Evans, 2009; Xiong et al., 2015), but see Tazoe et al., 2009). However, there is currently no physiological explanation to link the response of $g_m$ to $C_i$, and some concerns on the reliability of these measurements have been raised (Gu & Sun, 2014). We have implemented a $C_i$ response function which was derived empirically based on leaf-level measurements as shown in Figure S1.

$$f_4(C_i) = f_{min} + 1.5\left(1 - e^{(-C_i/38)}\right)e^{(-C_i/460)} \quad (5)$$

Equation (5) describes an abrupt increase of $g_m$ at low $C_i$ (until approx. 100 μmol/mol), and an exponential decline thereafter (Figure S1).

### 2.1.5 | Light response

The effect of absorbed radiation on $g_m$ and the underlying mechanisms driving this potential response are currently unresolved. Studies in which $g_m$ was measured at different light levels have reported either no clear responses of $g_m$ to variations in light (Loucos, Simonin, & Barbour, 2017; Tazoe et al., 2009; Yamori, Evans, & Caemmerer, 2010), or clear increases with light (Cai, Yang, Li, Wang, & Huang, 2017; Douthe, Dreyer, Brendel, & Warren, 2012; Yin et al., 2009) (see Figure S2). The following function was used to simulate the potential effects of light on $g_m$:

$$f_5(Q_a) = 1 - (1 - f_{min})\,e^{-0.003Q_a} \quad (6)$$

where $Q_a$ is absorbed photosynthetic photon flux density (μmol $m^{-2}$ $s^{-1}$). Equation (6) corresponds to a light response curve that takes the values of approximately $f_{min}$ and approximately 1 at $Q_a$ values of 0 and 1,500 μmol $m^{-2}$ $s^{-1}$, respectively (see Figure S2). The function corresponds to a steep increase of $g_m$ at low $Q_a$, a value of 0.8 (relative to $g_{m,max25}$) at approximately 500 μmol $m^{-2}$ $s^{-1}$ and a shallow response at high $Q_a$.

## 2.2 | C4 plants

In C4 plants, $g_m$ describes the conductance to $CO_2$ transfer from the intercellular airspace to the cytosol of the mesophyll cells, where the first binding of $CO_2$ occurs. Thus, the main difference to C3 plants is that the chloroplast components are not part of the diffusion pathway (von Caemmerer & Furbank, 1999). This means that $g_m$ in C4 plants causes a $CO_2$ concentration drawdown from $C_i$ to $C_m$, the $CO_2$ concentration in the mesophyll cytosol (i.e. $g_m = A_n/(C_i - C_m)$). Recent methodological advances have enabled measurements of $g_m$ in C4 plants (Barbour, Evans, Simonin, & Caemmerer, 2016; Ubierna, Gandin, Boyd, & Cousins, 2017). These measurements indicate that $g_m$ is higher in C4 plants than in C3 plants (see Figure 1). The response of $g_m$ to environmental factors was assumed to be identical to that in C3 plants (Equations (2)-(6)). This assumption could not be confirmed due to the scarcity of $g_m$ measurements in C4 plants, but recent studies indicate that the temperature as well as the $C_i$ response are qualitatively similar to that in C3 plants (Kolbe & Cousins, 2018; Ubierna et al., 2017). The relationship among C4 photosynthetic parameters was kept as in von Caemmerer and Furbank (1999) (see Table S1).

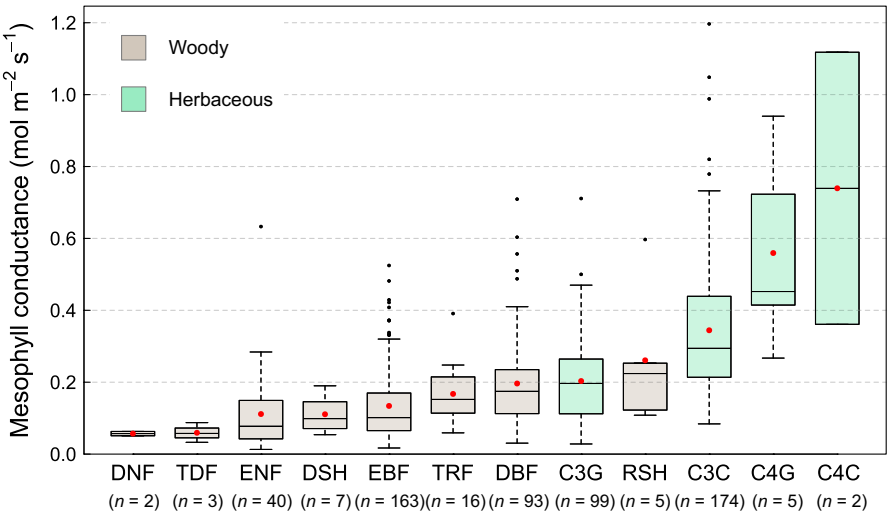


**FIGURE 1** Maximum (unstressed) mesophyll conductance values for different plant functional types (PFTs), standardized to 25°C. Horizontal lines within boxes represent medians, red dots represent means, the lower and upper boundaries of the boxes represent the first and third quantile, respectively, and whiskers represent 1.5 times the interquartile range. PFT abbreviations are: DNF = deciduous needle-leaf trees, TDF = tropical deciduous trees, ENF = evergreen needle-leaf trees, DSH = deciduous shrubs, EBF = evergreen broadleaf trees/shrubs, TRF = tropical evergreen trees, DBF = deciduous broadleaf trees, C3G = C3 herbs and grasses, RSH = raingreen shrubs, C3C = C3 crops, C4G = C4 grasses and herbs, C4C = C4 crops. Data presented here were not standardized to a given $C_i$ or to high light, and can be found in Appendix S3

## 2.3 | Implementation into the LSM JSBACH

The developed $g_m$ model was incorporated into the LSM JSBACH (Knauer et al., 2015; Reick et al., 2013), which is the land component of the MPI Earth system model (Giorgetta et al., 2013). Vegetation in JSBACH is classified into PFTs, which may co-occur in model grid cells as tiles, and which differ with respect to key physiological and biophysical properties. Fluxes and conductances are scaled to canopy-level with the LAI for each PFT, and the cover fraction-weighted mean of all tiles gives the respective grid cell value. Land-atmosphere water fluxes are calculated with a bulk transfer approach (Schulz, Dümenil, & Polcher, 2001). Canopy radiative transfer is modeled as described in Wang (2003) based on the model of Goudriaan (1977) and considers sun-lit and shaded canopy fractions in nine vertical layers. $g_s$ is modeled according to Medlyn et al. (2011) with PFT-specific stomatal slope parameters ($g_1$) taken from Lin et al. (2015) and a constant residual stomatal conductance ($g_0$) of 0.005 mol m$^{-2}$ s$^{-1}$. $A_n$ is simulated according to Farquhar, Caemmerer, and Berry (1980) and von Caemmerer and Furbank (1999) for C3 and C4 vegetation, respectively, and photosynthetic capacity is taken from Kattge, Knorr, Raddatz, and Wirth (2009), and if applicable re-calculated based on $N_a$ (leaf nitrogen per area) data in Kattge et al. (2011). In the photosynthesis routine of the model, $g_m$ is calculated first according to Equation (1), and $A_n$, $g_s$, $C_i$, and $C_c$ are subsequently solved iteratively. In the model versions where $g_m$ depends on $C_i$ (*ExpC* and *ExpCL*), $g_m$ is first calculated according to Equation (1) with $f_4$ set to 1 and then iteratively adjusted for $C_i$ (Equation (5)) in the same loop where $A_n$, $g_s$, $C_i$, and $C_c$ are solved.

## 2.4 | Maximum mesophyll conductance values ($g_{m,max25}$)

To parameterize the key parameter in the model, $g_{m,max25}$ (Equation 1), we compiled an extensive literature review of leaf-level $g_m$-measurements as described in Appendix S2. This dataset (Appendix S3) adds substantial new data to previous databases (e.g. Flexas et al., 2008) and comprises 609 individual $g_m$ measurements of 319 species from 295 studies. Measurements were performed using all common methods used to estimate $g_m$ (see e.g. Pons et al., 2009) and represent unstressed, fully expanded, and sun-exposed leaves. If necessary, measurements were converted to units of mol m$^{-2}$ s$^{-1}$ and standardized to 25°C using Equation (3). If $g_m$ was assumed to be light-dependent (model versions *ExpL* and *ExpCL*), measurements were standardized to high light (1,500 µmol m$^{-2}$ s$^{-1}$) according to Equation (6). If $g_m$ was assumed to be $C_i$ dependent (model versions *ExpC* and *ExpCL*), $g_{m,max25}$ was adjusted according to the $C_i$ measured along with $g_m$ (Equation 5). This adjustment accounts for the fact that different vegetation types operate at different $C_i/C_a$ (depending on the stomatal behavior in the model ($g_0$ and $g_1$ parameters) and the vapor pressure deficit (VPD)). The $g_m$ values were assigned to PFTs and the mean, median and standard error of the median were calculated (see Figure 1, Table 3).

## 2.5 | Adjustment of $C_i$-based to $C_c$-based photosynthetic parameters

The explicit representation of $g_m$ in photosynthesis models requires that photosynthetic parameters represent $C_c$-based

rather than $C_i$-based values, as the latter implicitly include the effects of $g_m$ (Ethier & Livingston, 2004). This typically requires that existing (i.e. $C_i$-based) parameters are adjusted to $C_c$-based parameters. Previous approaches for this parameter adjustment focused on the simultaneous derivation of $g_m$, $V_{cmax}$ and $J_{max}$ from $A_n - C_i$ curves using curve fitting techniques (Gu, Pallardy, Tu, Law, & Wullschleger, 2010; Sun, Gu, Dickinson, Pallardy et al., 2014). An alternative approach as applied in this study makes use of independent $g_m$ estimates which allow the conversion of $A_n - C_i$ curves to $A_n - C_c$ curves and the subsequent re-estimation of photosynthetic parameters on a $C_c$ basis. This alternative approach consists of three main steps (illustrated in Figure S3; R code available at https://bitbucket.org/juergenknauer/mesophyll_conductance):

1. Simulation of a PFT-specific $A_n - C_i$ curve under unstressed conditions, saturating light, and 25°C using the current (implicit $g_m$) photosynthesis routine of the model with $C_i$-based Rubisco parameters from Bernacchi et al. (2001). Under these conditions, $g_m$ is assumed to equal $g_{m,max25}$.
2. Calculation of $C_c$ from Fick's first law: $C_c = C_i - A_n/g_m$ and construction of the corresponding $A_n - C_c$ curve. Depending on whether $g_m$ is assumed to be independent of $C_i$ or not, $g_m$ is either assumed to be constant or a function of $C_i$ (Equation (5)).
3. Simultaneous fitting of $V_{cmax25}$ and $J_{max25}$ to the $A_n - C_c$ curve calculated in Step 2 using the same model as in step 1, but with $C_c$-based Rubisco parameters taken from Bernacchi et al. (2002). The fitting is done with a non-linear regression routine.

Compared to parameter adjustments based on measured $A_n - C_i$ curves, this approach has the advantage of being universally applicable across model types and model structures, and to both C3 and C4 photosynthesis models. This flexibility is achieved by an internally consistent parameter adjustment which is ensured by the employment of the exact same photosynthesis model and parameter values (e.g. leaf day respiration, Rubisco kinetic parameters) for both the parameter adjustment and the actual model simulations. In addition, this approach circumvents uncertainties associated with the determination of $g_m$ from $A_n - C_i$ curves (e.g. assignment of limitation states) by taking independent $g_m$ measurements. It follows that no raw data (i.e. $A_n - C_i$ curves) are required, but instead a sufficient number of $g_m$ measurements, from which representative estimates of $g_m$ can be inferred.

## 2.6 | Site-level simulations

The JSBACH model was run for eight eddy covariance sites within the FLUXNET network. The sites were selected to cover different PFTs and contrasting hydro-climates (Table 2). Meteorological data for all sites was downloaded from the FLUXNET2015 webpage (http://fluxnet.fluxdata.org/data/fluxnet2015-dataset/; accessed 2017-11-09).

**TABLE 2** Characteristics of eddy covariance sites used in this study

| Site | Vegetation type | Simulation period | MAT[a] (°C) | MAP[b] (mm) | Max. LAI | Vegetation height (m) | $V_{cmax25,Ci}$ (μmol m$^{-2}$ s$^{-1}$) | $g_{m,max25}$[c] (mol m$^{-2}$ s$^{-1}$) | Site reference |
|---|---|---|---|---|---|---|---|---|---|
| AT-Neu | C3 grasses/herbs | 2008–2012 | 6.3 | 852 | 6 | 0.5 | 70 | 0.197 | Wohlfahrt et al. (2008) |
| DE-Geb | C3 crops | 2005–2014 | 8.5 | 470 | 5 | 0.5 | 39 | 0.295 | Kutsch et al. (2010) |
| FI-Hyy | Evergreen needle-leaf forest | 1996–2014 | 3.8 | 709 | 3.3 | 14 | 41 | 0.090 | Vesala et al. (2005) |
| FR-LBr | Evergreen needle-leaf forest | 2003–2008 | 13.6 | 900 | 3.1 | 18 | 42 | 0.090 | Berbigier, Bonnefond, and Mellmann (2001) |
| FR-Pue | Evergreen broadleaf forest | 2005–2014 | 13.5 | 883 | 3.3 | 5.5 | 24 | 0.106 | Rambal et al. (2003) |
| GF-Guy | Tropical rainforest | 2006–2014 | 25.7 | 3,041 | 7 | 35 | 36 | 0.152 | Bonal et al. (2008) |
| US-Ha1 | Deciduous broadleaf forest | 1992–2012 | 6.6 | 1,071 | 4.9 | 23 | 45 | 0.176 | Urbanski et al. (2007) |
| US-Ne1 | C4 crops (irrigated maize) | 2002–2012 | 10.1 | 790 | 6 | 3 | 32 | 0.739 | Verma et al. (2005) |

[a]Mean annual temperature. [b]Mean annual precipitation. [c]Cover fraction-weighted $g_{m,max25}$ values of the plant functional types present at the site.

**TABLE 3** $g_{m,max25}$, $C_i$-based and $C_c$-based $V_{cmax25}$ and $J_{max25}$, and $J_{max25}/V_{cmax25}$ ratios for different plant functional types (PFTs) in the JSBACH model and for the *Exp* and *ExpC* model versions. Adjustments of $C_i$- to $C_c$-based parameters were performed as described in Section 2.5. $V_{cmax25,Ci}$ values were taken from Kattge et al. (2009), and if applicable re-calculated based on $N_a$ (leaf nitrogen per area) data in Kattge et al. (2011). PFT abbreviations are as in Figure 1.

| PFT | $g_{m,max25}$ ± SEM (mol $m^{-2}$ $s^{-1}$) | $V_{cmax25,Ci}$ (µmol $m^{-2}$ $s^{-1}$) | $J_{max25,Ci}$ (µmol $m^{-2}$ $s^{-1}$) | $J_{max25,Ci}/V_{cmax25,Ci}$ | $V_{cmax25,Cc}$ (µmol $m^{-2}$ $s^{-1}$) | $J_{max25,Cc}$ (µmol $m^{-2}$ $s^{-1}$) | $J_{max25,Cc}/V_{cmax25,Cc}$ | $g_{m,max25}$[a] (mol $m^{-2}$ $s^{-1}$) | $V_{cmax25,Cc}$ (µmol $m^{-2}$ $s^{-1}$) | $J_{max25,Cc}$ (µmol $m^{-2}$ $s^{-1}$) | $J_{max25,Cc}/V_{cmax25,Cc}$ |
|---|---|---|---|---|---|---|---|---|---|---|---|
| | *Exp* | *Imp* | *Imp* | *Imp* | *Exp* | *Exp* | *Exp* | *ExpC* | *ExpC* | *ExpC* | *ExpC* |
| DNF | 0.057 ± 0.008 | 33.1 | 62.9 | 1.9 | 59.3 | 65.0 | 1.10 | 0.054 | 68.1 | 89.9 | 1.32 |
| TDF | 0.058 ± 0.020 | 31.0 | 58.9 | 1.9 | 49.8 | 60.4 | 1.21 | 0.056 | 50.4 | 76.9 | 1.41 |
| ENF | 0.078 ± 0.021 | 52.7 | 100.1 | 1.9 | 118.8 | 105.5 | 0.89 | 0.074 | 113.3 | 145.3 | 1.28 |
| DSH | 0.098 ± 0.025 | 49.8 | 94.7 | 1.9 | 75.7 | 96.9 | 1.28 | 0.100 | 78.1 | 112.1 | 1.44 |
| EBF | 0.101 ± 0.010 | 61.4 | 116.7 | 1.9 | 117.8 | 121.1 | 1.03 | 0.100 | 126.7 | 167.4 | 1.32 |
| TRF | 0.152 ± 0.026 | 39.0 | 74.1 | 1.9 | 42.1 | 74.1 | 1.76 | 0.151 | 43.7 | 76.9 | 1.76 |
| DBF | 0.175 ± 0.016 | 52.1 | 98.9 | 1.9 | 58.6 | 99.2 | 1.69 | 0.172 | 61.3 | 104.2 | 1.70 |
| C3G | 0.197 ± 0.015 | 50.1 | 95.2 | 1.9 | 54.0 | 95.1 | 1.76 | 0.198 | 55.8 | 98.7 | 1.77 |
| RSH | 0.224 ± 0.111 | 49.8 | 94.7 | 1.9 | 52.1 | 94.4 | 1.81 | 0.230 | 53.6 | 97.3 | 1.82 |
| C3C | 0.295 ± 0.017 | 80.2 | 152.4 | 1.9 | 87.9 | 152.5 | 1.73 | 0.305 | 90.3 | 158.5 | 1.76 |
| | | $V_{pmax25,Ci}$ (µmol $m^{-2}$ $s^{-1}$) | | | $V_{pmax25,Cc}$ (µmol $m^{-2}$ $s^{-1}$) | | | | $V_{pmax25,Cc}$ (µmol $m^{-2}$ $s^{-1}$) | | |
| C4G | 0.452 ± 0.151 | 40.0 | | | 118.9 | | | 0.382 | 189.0 | | |
| C4C | 0.739 ± 0.474 | 60.0 | | | 145.4 | | | 0.620 | 193.6 | | |

SEM: standard error of the median.

[a]Standardized to a $C_i$ of 260 µmol $mol^{-1}$ (Equation (5)).

All sites were run with meteorological forcing from the flux towers. Vegetation height, roughness length, and LAI were adjusted according to values reported in the literature, and $C_i$-based photosynthetic capacity ($V_{cmax25,Ci}$ and $J_{max25,Ci}$) was adjusted to match the flux measurements. For all sites, all model versions (*Imp*, *Exp*, *ExpC*, *ExpL*, *ExpCL*) were forced with (1) observed meteorological conditions and (2) elevated $CO_2$ concentrations (ambient + 200 μmol/mol), and the same meteorological forcing as in the ambient $CO_2$-runs.

### 2.7 | Global simulations

To investigate the large-scale implications of an explicit representation of $g_m$ in JSBACH, we conducted global runs for the *Imp*, *Exp*, and *ExpCL* model versions under historical (1970–2004) and projected future conditions (2070–2099). Bias-corrected daily meteorological forcing (0.5° spatial resolution) for both the historical and future runs was obtained from the Inter-Sectoral Impact Model Intercomparison Project (ISIMIP) (Frieler et al., 2017; Hempel, Frieler, Warszawski, Schewe, & Piontek, 2013), using output from the HadGEM2-ES model (Martin et al., 2011). Future runs were conducted with RCP4.5 and RCP8.5 scenarios. Land cover was obtained from Pongratz, Reick, Raddatz, and Claussen (2007) and assumed to be unchanged in the historical and future runs. $g_{m,max25}$ as well as $V_{cmax25}$ and $J_{max25}$ values are listed in Table 3.

## 3 | RESULTS

### 3.1 | Unstressed $g_m$ values across PFTs

Figure 1 shows the results of the literature review, revealing distinct patterns in unstressed $g_m$ across PFTs. Lowest values were found in needle-leaf and evergreen broadleaf trees, followed by tropical evergreen trees and deciduous broadleaf trees. Generally, herbaceous species had higher $g_m$ values than woody species. Within herbaceous PFTs, crops had higher $g_m$ values than grasses and wild herbs, and C4 plants had higher values than C3 plants. The number of measurements was unequally distributed among the PFTs and 87% of all measurements were performed in only four PFTs (C3C, EBF, C3G, DBF). It follows that most PFTs are poorly sampled and the corresponding $g_m$ measurements are less robust than in the well-sampled PFTs. However, the four highly sampled PFTs also showed a large spread, reflecting the wide range of $g_m$ values among measurement methods or among different species within each PFT. Results in Figure 1 show $g_m$ values that were not standardized to a given $C_i$ or to high light. Accounting for a potential response of $g_m$ to light or $C_i$ led to only minor changes in the magnitude of $g_m$ and its pattern across PFTs (Table 3 and Table S2).

### 3.2 | Parameter adjustment

The required parameter adjustment procedure as described in Section 2.5 led to significant changes to the two key photosynthetic parameters in the model, $V_{cmax25}$ and $J_{max25}$ (Table 3). The $C_c$-based parameters ($V_{cmax25,Cc}$ and $J_{max25,Cc}$) account for the lower available $CO_2$ concentration due to the effects of $g_m$, and are thus usually higher than their $C_i$-based counterparts. For all PFTs, $V_{cmax25}$ was more strongly affected than $J_{max25}$, which resulted in a decrease of the $J_{max25}/V_{cmax25}$ ratio. The difference between the $C_i$-based and $C_c$-based parameters depends both on the magnitude of $g_m$ and the magnitude of $V_{cmax25,Ci}$ and $J_{max25,Ci}$, and is highest when $g_m$ is low and photosynthetic capacity is high (as e.g. in ENF). Thus, effects are strongest when the $CO_2$ drawdown from the intercellular airspaces to the chloroplasts ($C_i - C_c$) is high. The decrease of the $J_{max25,Cc}/V_{cmax25,Cc}$ ratio led to a shift of the inflection point (the $C_i$ where photosynthetic limitation changes from Rubisco-limited to RuBP (ribulose-1,5-bisphosphate)-limited) to lower $C_i$, which is associated with a higher fraction of photosynthesis occurring in the electron transport-limited domain (see e.g. Figure S3).

In the model versions where $g_m$ is affected by $C_i$ (*ExpC* and *ExpCL*), $g_m$ was assumed to change throughout the $A_n - C_i$ curve according to Equation (5), that means it increases sharply at low $C_i$ and decreases continuously thereafter. When accounting for this potential response, the re-adjusted photosynthetic parameters, in particular $J_{max25,Cc}$, were considerably higher compared to the default version (*Exp*). The higher $J_{max25,Cc}$ compensates for the low $g_m$ simulated at higher $C_i$ where RuBP-regeneration is limiting (Figure S1), and thus maintains the same $A_n$ at high $C_i$ as in the implicit case. *ExpC* and *ExpCL* were thus characterized by significantly higher $J_{max25,Cc}/V_{cmax25,Cc}$ ratios compared to the *Exp* model version (Table 3). The model versions accounting for a light response of $g_m$ (*ExpL* and *ExpCL*) did generally not show strong deviations from the corresponding versions without a light response (*Exp* and *ExpC*, respectively), but tended to have lower $V_{cmax25,Cc}$ values and slightly higher $J_{max25,Cc}/V_{cmax25,Cc}$ ratios (Table S2).

In the C4 photosynthesis model described by von Caemmerer and Furbank (1999), the only parameter affected by the parameter adjustment is the maximum PEP-carboxylation rate ($V_{pmax25}$) (Figure S4). In case of a $g_{m,max25}$ of 0.739 mol $m^{-2}$ $s^{-1}$, the median value observed in C4 crops, $V_{pmax25}$ increased strongly from 60 ($C_i$-based) to approximately 145 μmol $m^{-2}$ $s^{-1}$ ($C_m$-based; Table 3).

### 3.3 | Effects on simulated leaf-level photosynthesis

Simulated photosynthesis in the implicit (*Imp*) and the explicit (*Exp*) model versions are compared in Figure 2. Shown are $A_n - C_i$ curves calculated from leaf-level simulations under contrasting temperature and light conditions. The adjustment of $V_{cmax25}$ and $J_{max25}$ was always performed under reference conditions (i.e. temperature of 25°C and saturating light) and aimed to minimize the difference between the implicit and explicit simulations under these reference conditions (Figure 2a, solid lines). The achieved goodness of fit depends on the magnitude of $g_m$, with lower $g_m$ resulting in a poorer fit to the implicit $A_n - C_i$ curve under otherwise equal conditions (Table S3). Importantly, when temperature and light deviate from the reference conditions, the agreement between the implicit and explicit model deteriorates. This is especially relevant when temperature changes,

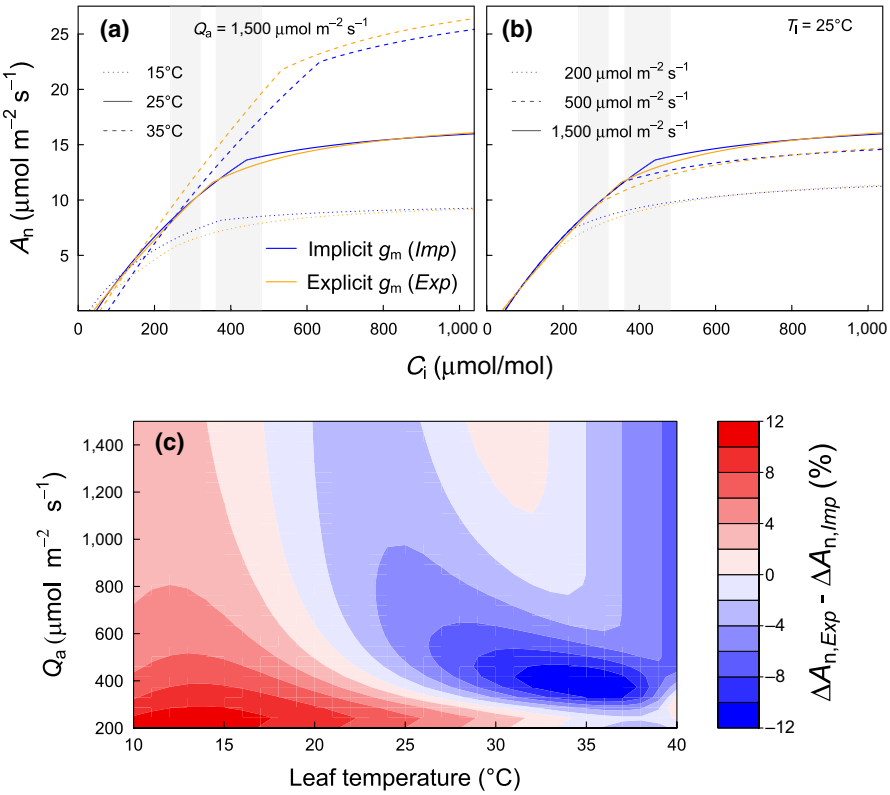


**FIGURE 2** (a) $A_n$ – $C_i$ curves for the implicit (*Imp*, blue) and explicit (*Exp*, orange) model versions for three different temperatures (b) and light conditions and (c) the resulting differences in photosynthetic sensitivity to $CO_2$ between the implicit and the explicit model version for the grey shaded $C_i$ regions in (a) and (b). $\Delta A_n$ in (c) is defined as $\Delta A_n = (A_{n,eCO2} - A_{n,aCO2})/A_{n,aCO2} \times 100$, where $aCO_2$ denotes the intercellular $CO_2$ concentration ($C_i$) range between 240 and 320 µmol/mol (=0.6 × 400 – 0.8 × 400 µmol/mol) and $eCO_2$ denotes the $C_i$ range between 360 and 480 µmol/mol (=0.6 × 600 – 0.8 × 600 µmol/mol). Positive values in (c) indicate that $A_n$ in the explicit model is more sensitive to $CO_2$ than $A_n$ in the implicit model, negative values indicate the opposite. Shown are leaf-level simulations using the C3 photosynthesis model described in Farquhar et al. (1980) with the following parameters: $V_{cmax25,Ci}$ = 40 µmol m$^{-2}$ s$^{-1}$; $J_{max25,Ci}$ = 76 µmol m$^{-2}$ s$^{-1}$; $g_{m,max25}$ = 0.1 mol m$^{-2}$ s$^{-1}$; $V_{cmax25,Cc}$ = 50.8 µmol m$^{-2}$ s$^{-1}$; $J_{max25,Cc}$ = 76.86 µmol m$^{-2}$ s$^{-1}$; $R_l$ (respiration rate in light) = 0.44 µmol m$^{-2}$ s$^{-1}$; and Rubisco kinetic parameters as listed in Table S1

because $g_m$ exhibits a strong temperature response (Equation (3)), leading to higher and lower $A_n$ at temperatures higher and lower than 25°C, respectively (Figure 2a). The model comparison at lower light conditions (Figure 2b) did not necessarily lead to a poorer agreement between the model versions, but the comparison exemplifies that the mismatch between the model versions and thus the sensitivities to $CO_2$ strongly depends on the prevailing conditions. The *ExpC* model led to similar curves as shown in Figure 2 (Figure S6). Assuming that $g_m$ responds to light (*ExpL*) led to much lower simulations of $A_n$ under low light, as well as to higher sensitivities to rising $CO_2$ throughout the whole $C_i$ range (Figure S7). The deviations between the implicit and explicit model versions caused changes in the relative sensitivity of $A_n$ to changes in $C_i$ compared to the reference conditions (Figure 2c). In general, $A_n$ showed a stronger relative response to $C_i$ in the explicit compared to the implicit model at lower temperatures, but the opposite behavior at high temperatures. Note that Figure 2c depicts changes in the sensitivity of $A_n$ to $C_i$ in relative terms (see Figure caption), which was decreased at high temperatures despite similar slopes of $A_n$ – $C_i$ in Figure 2a. These contrasts were more pronounced at lower light conditions. It has to be noted that the sensitivities and their relation between the implicit and explicit model version depend on the $C_i$ range of interest (shaded areas in Figure 2a,b), which explains the fact that the $CO_2$ effect of $g_m$ as shown in Figure 2c becomes negative already at temperatures lower than 25°C at high $Q_a$.

### 3.4 | Site-level simulations

The integrated response of ecosystem-level $A_n$ ($A_{n,canopy}$) and $g_s$ (canopy conductance, $G_c$) to changes in atmospheric $CO_2$ concentrations are analyzed in Figure 3 for an exemplary set of ecosystems from the FLUXNET2015 database. In the implicit model version (*Imp*), $A_{n,canopy}$ increased under $eCO_2$ at all sites with C3 vegetation. The relative increases depend on temperature as described previously (Kirschbaum, 1994), and were more pronounced in warm (e.g. GF-Guy) than in cold climates (e.g. FI-Hyy). The explicit model version that does not consider a light and $C_i$ response (*Exp*) showed higher sensitivities of $A_{n,canopy}$ to $eCO_2$ for most sites, but a significantly lower sensitivity for GF-Guy, which can be explained by the lower photosynthetic sensitivity to $CO_2$ at higher temperatures (Figure 2).

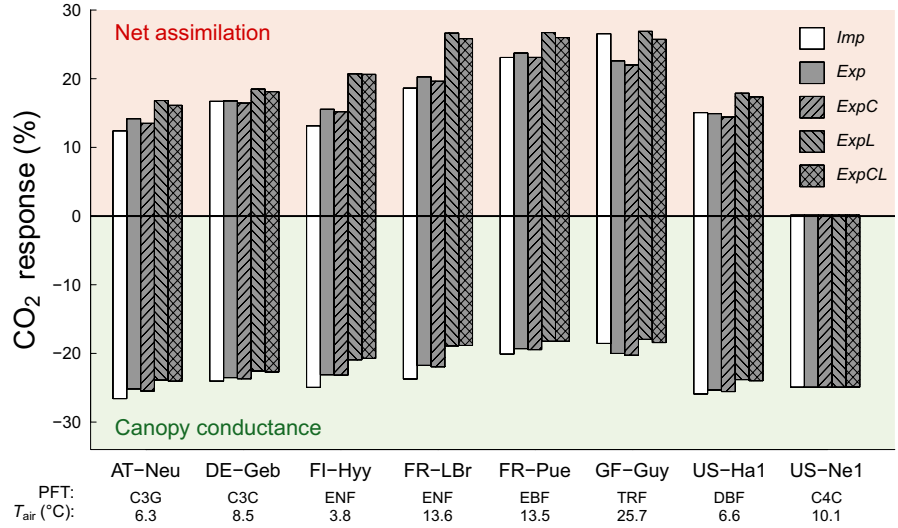


**FIGURE 3** Relative responses of ecosystem-level net assimilation and canopy conductance to elevated atmospheric $CO_2$ concentrations for the five main model versions tested in this study (*Imp* = implicit $g_m$; *Exp* = explicit $g_m$; *C* = $C_i$ response of $g_m$; *L* = light response of $g_m$). $CO_2$ response is calculated as $(X_{eCO2} - X_{aCO2})/X_{aCO2} \times 100$, where X denotes either canopy net assimilation or canopy conductance, and $aCO_2$ and $eCO_2$ denote ambient and elevated (ambient + 200 μmol/mol) atmospheric $CO_2$ concentrations, respectively. PFT abbreviations are as in Figure 1. $T_{air}$ represents the mean annual temperature (see also Table 2)

The model configuration that responds to $C_i$, but not to $Q_a$ (*ExpC*) showed similar or slightly lower responses compared to the *Exp* model version, which is likely due to the fact that the lower simulated $g_m$ was largely compensated by the higher $C_c$-based photosynthetic capacity (Table 3). In contrast, model configurations that simulate a response of $g_m$ to light (*ExpL* and *ExpCL*) showed the highest responsiveness of $A_{n,canopy}$ to $CO_2$, which is a consequence of the continuously higher sensitivity under low light in the *ExpL* and *ExpCL* versions due to the marked decrease of $g_m$ at low light (Equation (6), Figure S7). This effect is amplified at the canopy level, as a considerable fraction of a closed canopy continuously operates at low light conditions.

The positive responses in $A_{n,canopy}$ were accompanied by negative responses in $G_c$, that is stomatal closure. A consistent pattern in Figure 3 is the opposite response of $G_c$ compared to $A_{n,canopy}$ in the sense that a stronger response of $A_{n,canopy}$ was associated with a weaker response of $G_c$, with the result that the response of ecosystem-level intrinsic water-use efficiency ($iWUE_{,canopy} = A_{n,canopy}/G_c$) to $eCO_2$ did not vary among the model runs (i.e. it always increased by the same amount). This can be explained as an intrinsic property of the stomatal model employed here (Medlyn et al., 2011), in which $C_i/C_a$ is assumed to stay constant with rising $CO_2$ concentrations. This model behavior is unchanged in the explicit model version with the consequence that stronger positive responses of $A_n$ to $eCO_2$ are accompanied by weaker decreases in $g_s$, the combination of which keeps $C_i/C_a$ constant. Hence, the changes in $g_s$ are not direct effects of $g_m$, but indirect ones via $A_n$ that are caused by the coupling between $A_n$ and $g_s$ in the model. This relationship holds regardless of whether $g_m$ is assumed to stay constant or to decrease over time, as it is the case in the *ExpC* model runs.

For C4 plants, none of the explicit model versions led to any changes in simulations of $A_{n,canopy}$ and $G_c$ compared to the implicit model. All model runs did not show a response of $A_{n,canopy}$ to $eCO_2$, and a constant decrease of c. 25% in $G_c$. The reason for this is that $C_i$ did not fall in the range where photosynthesis is limited by $V_{pmax}$ (e.g. low $C_i$). This behavior depends on the parameterization of the model, and $g_m$ effects might be more important under conditions of water stress.

As shown in Figure 2, the fact that $g_m$ responds to temperature leads to a significantly different temperature response of $A_{n,canopy}$. It follows that the photosynthetic sensitivity to $CO_2$ shows a different response to temperature in the explicit compared to the implicit model versions (Figure 4). The sensitivity of $A_{n,canopy}$ to $CO_2$ increased with temperature in all model versions, but with a different functional response (i.e. slope). In particular at low temperatures (<20°C), the explicit model versions simulated a higher photosynthetic sensitivity to $CO_2$ compared to the implicit version. This behavior was reversed at approx. 20°C, above which *Exp* and *ExpC* simulated a lower photosynthetic sensitivity to $CO_2$ compared to *Imp*. The *ExpL* version showed the highest sensitivity at low temperatures due to the above mentioned amplification of the light response at canopy level. At high temperatures (above c. 25°C), *ExpL* and *Imp* showed similar temperature sensitivities.

As demonstrated in Figures 2–4, the effects of $g_m$ on the photosynthetic responses to $eCO_2$ depend not only on the magnitude of $g_m$ (and thus PFT) but also on the environmental conditions, foremost temperature and radiation. To investigate the isolated effects of $g_m$ without any confounding meteorological factors, we conducted additional ecosystem-level simulations for the sites US-Ha1 and GF-Guy, in which $g_{m,max25}$ was varied while keeping the climate forcing unchanged. For these simulations, $g_{m,max25}$ was reduced

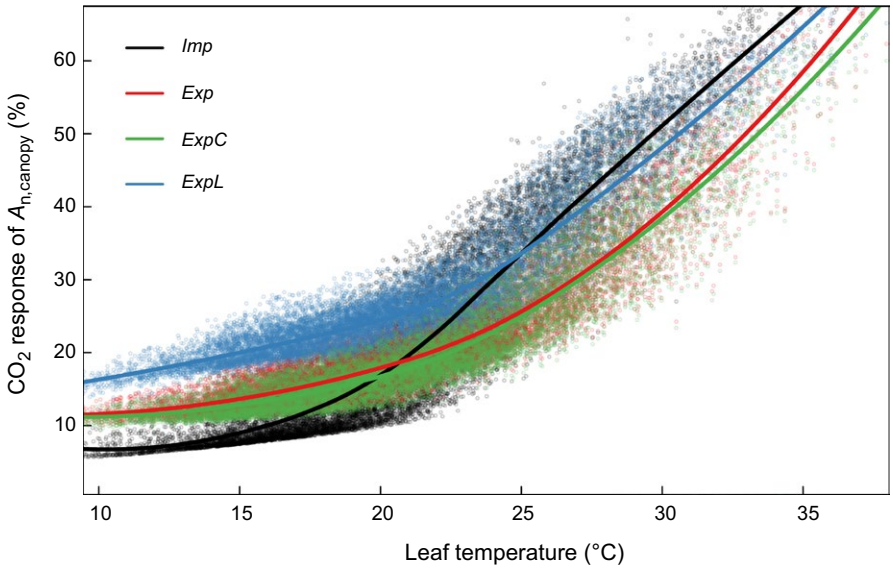


**FIGURE 4** Sensitivity of canopy-level net assimilation ($A_{n,canopy}$) to elevated $CO_2$ concentrations in the implicit (*Imp*) and explicit model versions (*Exp*, *ExpC*, *ExpL*) for the Mediterranean pine forest site FR-LBr. $CO_2$ response of $A_{n,canopy}$ is defined as $(A_{n,canopy,eCO2} - A_{n,canopy,aCO2})/A_{n,canopy,aCO2} \times 100$, where $aCO_2$ and $eCO_2$ denote ambient and elevated (ambient + 200 μmol/mol) atmospheric $CO_2$ concentrations, respectively. Data were filtered to represent periods in the growing season (four most productive months), at daytime ($Q_a$ > 200 μmol $m^{-2}$ $s^{-1}$), and in the absence of soil water stress (β > 0.95; Equation (4)). Points are half-hourly simulation results, and lines indicate local polynomial regression fits (loess) to the points

stepwise from 10,000 (i.e. non-limiting) to 0.075 mol $m^{-2}$ $s^{-1}$, and $V_{cmax25}$ and $J_{max25}$ were re-adjusted for each change in $g_{m,max25}$ as described in Section 2.5. The results demonstrate that the effects of $g_m$ on simulations of photosynthesis strengthen when its magnitude decreases (Figure 5). This is a consequence of the increasing mismatch between the implicit and explicit model versions when $g_m$ decreases (Table S3), an effect that amplifies when conditions deviate from those that were used for the parameter adjustment (Figure 2). In the *Exp* model version, the high temperatures in the tropical site GF-Guy thus caused the photosynthetic sensitivity to $CO_2$ to decrease when $g_m$ decreases, whereas the opposite was the case in the temperate site US-Ha1. The *ExpL* version caused a stronger sensitivity with decreasing $g_m$ for all sites. At US-Ha1, this led to a significant increase of the photosynthetic sensitivity to $CO_2$ at low $g_m$. At GF-Guy, in contrast, a potential light response of $g_m$ offsets the increase caused by a reduced $g_m$, with the consequence that the *ExpL* model version showed a similar sensitivity for all $g_m$ values.

At both sites, the proportion of Rubisco-limited $A_{n,canopy}$ decreased when $g_{m,max25}$ decreased. Again, this is a consequence of the parameter adjustment (see Section 2.5), in which the stronger changes in $V_{cmax25}$ compared to $J_{max25}$ lead to a shift of the inflection point to a lower $C_i$, which is associated with a higher fraction of photosynthesis occurring in the RuBP regeneration-limited domain. This effect (i.e. the change in $J_{max25}/V_{cmax25}$) increases with a decrease in $g_m$ under otherwise equal conditions. In general, this shift towards lower proportions of Rubisco-limited photosynthesis on total canopy level photosynthesis counteracts the higher photosynthetic sensitivity to $CO_2$ caused by an explicit $g_m$, as photosynthesis in the RuBP regeneration limited region shows a lower sensitivity to rising $CO_2$ concentrations.

## 3.5 | Global simulations

At the global scale, the widespread substantial increases in mean annual GPP from the historical (1975–2004) to the future RCP8.5 (2070–2099) simulation illustrate the commonly observed $CO_2$-fertilization effect (Figure 6a). Exceptions from this upward trend were found in some semi-arid regions, as well as in parts of the Amazon basin, which experience a drying trend in the climate projections by HadGEM2-ES. Transpiration (Figure 6b), showed weaker absolute responses and a more diverse pattern throughout the globe. In contrast to GPP, transpiration tended to be reduced due to stomatal closure, but this reduction may be offset by increasing VPD in some regions of the earth (Kala et al., 2016). The more moderate RCP4.5 future scenario showed similar patterns, but smaller absolute differences (Figure S8). Figure 6 further reveals that $g_m$ had spatially contrasting effects on the photosynthetic sensitivity to $CO_2$. The differences in the Δ values between the *Exp* and the *Imp* version largely reflect both the magnitude of $g_m$ (and thus vegetation type), and the environmental conditions as described earlier. It follows that the largest changes could be found in high latitudes, in particular in boreal forests, which show a combination of vegetation with a low $g_m$ (ENF and DNF) and a cool climate, both of which increased the photosynthetic sensitivity to $CO_2$ when $g_m$ is modeled explicitly. Changes were moderately positive throughout large parts of the temperate (+5% to + 15%) and semi-arid regions of the earth (+0% to + 5%) and slightly

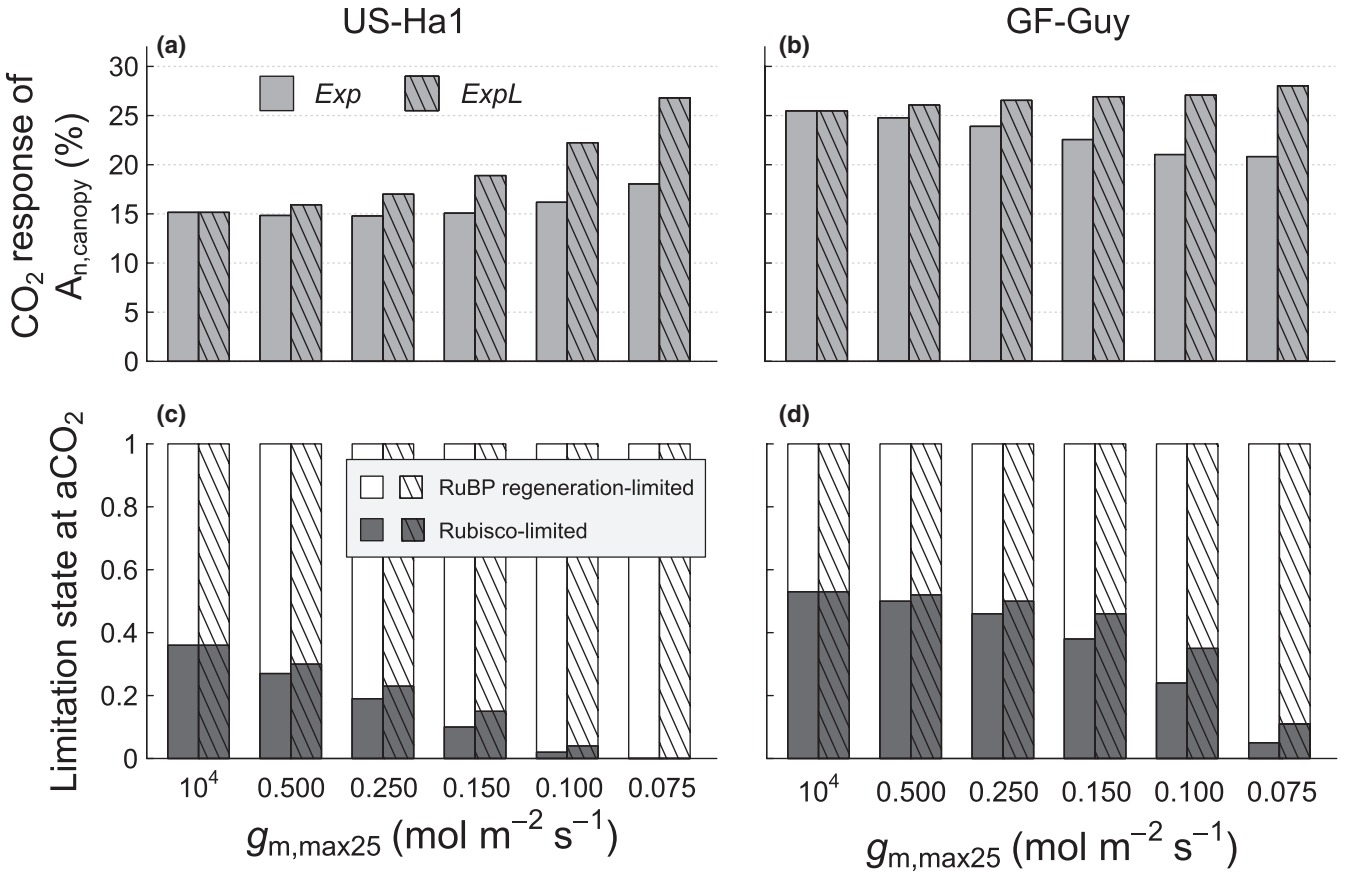


**FIGURE 5** Site-level simulations for the sites US-Ha1 and GF-Guy with differing values of $g_{m,max25}$. (a–b) $CO_2$ response of $A_{n,canopy}$ (defined as in Figure 3). (c–d) Fraction of canopy level net assimilation ($A_{n,canopy}$) limited by the two limitation states of the photosynthesis model in the ambient $CO_2$ ($aCO_2$) simulations. $V_{cmax25}$ and $J_{max25}$ were re-adjusted for each $g_{m,max25}$ value as described in Section 2.5

negative in large parts of the inner tropics (−2% to 0%). This decrease in the $CO_2$ sensitivity of photosynthesis is in accordance with the site-level results, and is mostly attributable to the high temperatures in these regions (Figure 2). The *ExpCL* model version (Figure 6e,f) showed similar spatial patterns as the *Exp* model, but consistently stronger positive responses. The reason for the stronger response is the light response function that amplifies at canopy level, as described earlier. The changes in transpiration in both the *Exp* and *ExpCL* model versions mirror those found for GPP, but are generally weaker. The weaker responses of transpiration compared to GPP are likely caused by aerodynamic decoupling, that cause a lower sensitivity of modeled transpiration to atmospheric $CO_2$ compared to $G_c$ (Knauer et al., 2017).

The differences among plant types are more clearly demonstrated in Figure 7 (for the RCP8.5 scenario; see Figure S9 for the RCP4.5 scenario). As stated earlier, the differences among the PFTs are not only caused by differences in $g_m$, but also by differences in the prevailing climatic conditions. For example, the lower response of TDF compared to DNF, despite similar $g_{m,max25}$ values, can be attributed to the higher temperatures the TDF are exposed to (Figure 4). Nonetheless, the comparison of co-occurring PFTs in the same model grid cells (i.e. PFTs experiencing identical climate forcing), showed significant differences in the simulated photosynthetic sensitivity, indicating that changes therein can primarily be attributed to differences in $g_m$, and not to climate (Figure S10).

The widespread increases in plant carbon uptake in the explicit model versions relative to the implicit version of 5%–25% between 1975–2004 and 2070–2099 (Figures 6 and 7) are reflected in the clear increases in simulations of global GPP (Figures S11–S13). Differences in the simulated global GPP values in the RCP8.5 scenario between the *Imp* and the *Exp* and *ExpCL* model versions amounted to 3.6 and 6.6 Pg C $yr^{-1}$, respectively, for the 2070–2099 period. In both cases, about two-third of the increase was caused by regions north of 30°N (Figure S11), in particular in boreal forests (Figure 7).

## 4 | DISCUSSION

### 4.1 | Required adjustments to the Farquhar et al. (1980) photosynthesis model

The explicit consideration of $g_m$ in models of photosynthesis requires that photosynthetic parameters are adjusted from their apparent ($C_i$-based) to true ($C_c$-based) values, as the former implicitly account for the effects of $g_m$. The Rubisco kinetic parameters ($K_o$, $K_c$ and $\Gamma^*$) as well as their activation energies have been determined by for exmaple Bernacchi et al. (2002) on a $C_c$ basis.

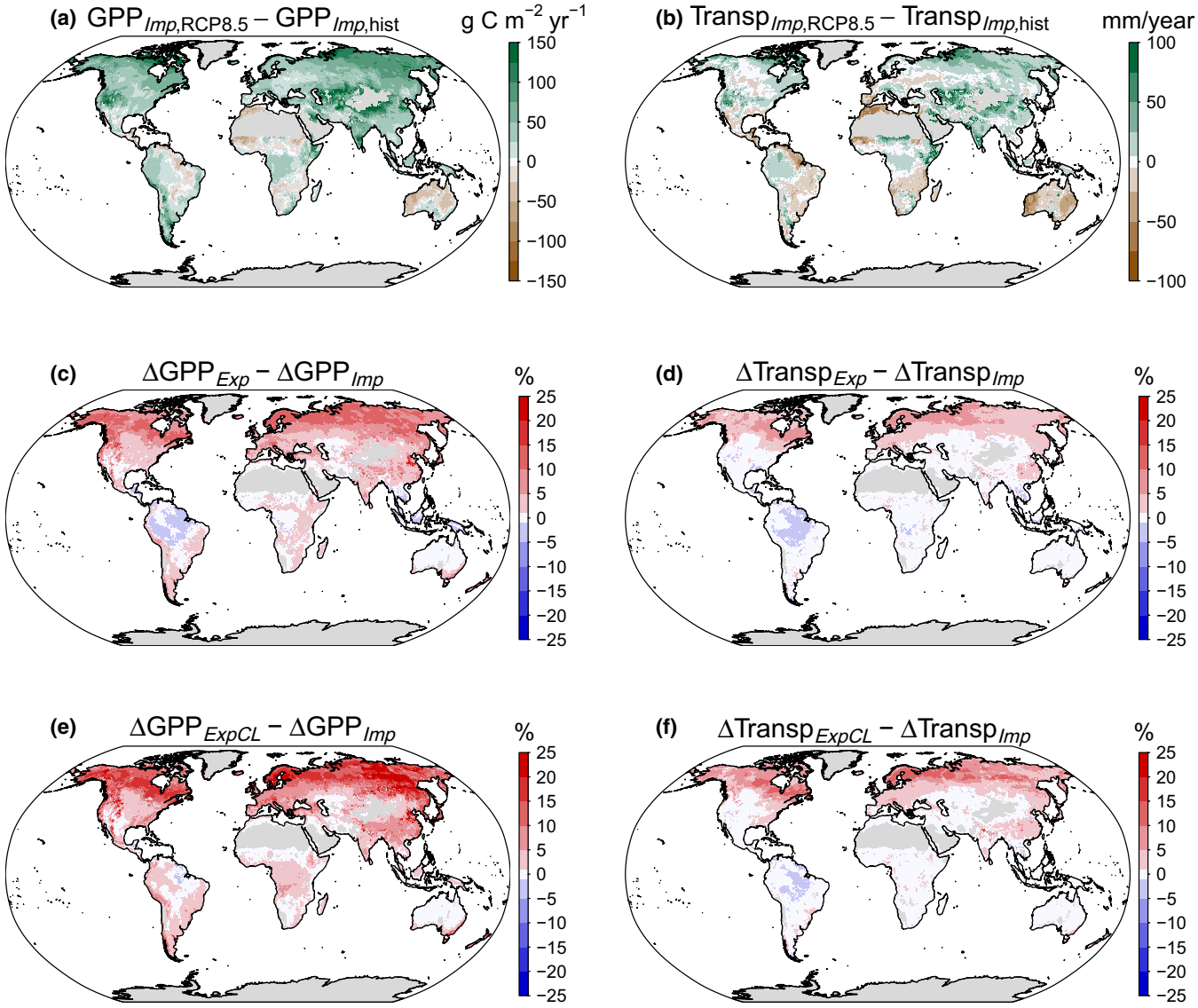


**FIGURE 6** (a–b) Simulated differences between the RCP8.5 future scenario (2070–2099) and the historical (hist) runs (1975–2004) in mean annual gross primary productivity (GPP) and Transpiration (Transp) in the implicit (*Imp*) model version. (c–f) Relative differences between the *Imp* and the *Exp* (c–d) and *ExpCL* (e–f) model versions. Δ is defined as $\Delta = (X_{RCP8.5} - X_{hist})/X_{hist} \times 100$, where X is either GPP or Transpiration. Regions with an average annual GPP < 200 g C $m^{-2}$ $yr^{-1}$ were masked out. Red colors in panels c–f denote stronger increases in GPP or Transpiration in the $g_m$-explicit simulations compared to the $g_m$-implicit simulations

These parameters are commonly assumed to be conserved across C3 plants (but see e.g. Walker et al., 2013), which leaves the species-specific parameters $V_{cmax25}$ and $J_{max25}$ left to adjust. Here, we suggest a simple and flexible parameter adjustment scheme that is applicable across model representations of photosynthesis (Figures S3–S5) and that does not require measured $A_n - C_i$ curves, but instead independent $g_m$ estimates. The approach ensures that $V_{cmax25}$ and $J_{max25}$ are converted in accordance with the individual structure and parameterization of the photosynthesis model. This consistency of $V_{cmax25,Cc}$ and $J_{max25,Cc}$ with the other parameters in the model (e.g. Rubisco kinetics) could not be assured if $V_{cmax25,Cc}$ and $J_{max25,Cc}$ were taken directly from leaf-level measurements, as these values are often derived assuming different photosynthetic parameters than the model (see Table S4 for a sensitivity analysis). It should be noted that the original $C_i$-based estimates of $V_{cmax}$ and $J_{max}$ might not represent $A_n - C_i$ curves well due to the assumption of an infinite $g_m$ (Ethier & Livingston, 2004). Any potential bias inherent in the $C_i$-based parameters will be propagated to their $C_c$-based values (Table 3). However, the degree of bias in the $C_i$-based parameters as well as the actual implications for the derived $C_c$-based parameters still needs to be investigated.

The adjustment from apparent to true values resulted in changes to the key parameters $V_{cmax25}$ and $J_{max25}$ that are qualitatively comparable to the results of previous adjustments (Sun, Gu, Dickinson, Pallardy et al., 2014), and that compare well with independently adjusted parameters by Bahar, Hayes, Scafaro, Atkin, and Evans (2018)

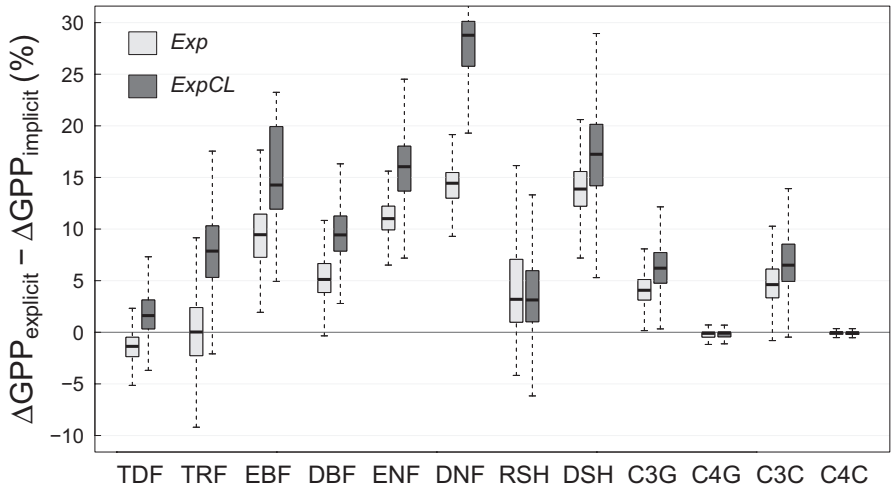


**FIGURE 7** Photosynthetic sensitivity to future climate conditions for different plant functional types (PFTs), expressed as the differences between the ΔGPP of the explicit (*Exp* or *ExpCL*) and implicit (*Imp*) $g_m$ model versions. ΔGPP was calculated as ($\Delta GPP = GPP_{RCP8.5} - GPP_{hist}$)/$GPP_{hist} \times 100$, where $GPP_{RCP8.5}$ and $GPP_{hist}$ denote GPP simulated in the RCP8.5 future scenario (2070–2099) and the historical runs (1975–2004), respectively. Shown are results at tile-level (i.e. GPP is simulated only for the respective PFT and not for the entire grid cell) and only for grid cells where the cover fraction of the respective PFT was at least 30%. PFT abbreviations are as in Figure 1

(results not shown). The adjustment again underlines the asymmetrical effects that $g_m$ has on $V_{cmax25}$ and $J_{max25}$. The stronger change in $V_{cmax25}$ compared to $J_{max25}$ as a result of the re-adjustment decreases the $J_{max25}/V_{cmax25}$ ratio and shifts the inflection point towards lower $C_i$ values. In general, these changes to the photosynthesis model result in an altered response of photosynthesis to key environmental factors like temperature and light. Further, it also changes the sensitivity of photosynthesis to $eCO_2$ in dependence on the environmental conditions. This can mostly be attributed to the fact that the parameter adjustment is performed under reference conditions of 25°C and saturating light. Under these conditions, the agreement between the explicit and implicit model versions is the best, but it deteriorates when conditions deviate from the reference conditions, an effect that was previously asserted by Sun, Gu, Dickinson, Norby et al. (2014). Most relevant in this context is the strong temperature response of $g_m$ (Equation (3)), which leads to a significant deviation of simulated photosynthesis under higher and lower temperatures in the explicit model version. It may be noted that these introduced deviations could be avoided by additionally re-adjusting the activation energy of $V_{cmax,Cc}$. This would, however, not be in accordance with the adjustment of the Rubisco kinetic parameters as performed in Bernacchi et al. (2002), where changes in the temperature response of $A_n$ were entirely attributed to $K_c$ and $K_o$, thereby assuming an unchanged activation energy of $V_{cmax}$. This approach is also justified theoretically since $V_{cmax,Cc}$, the substrate-saturated photosynthesis rate, is by definition unaffected by $g_m$. We thus argue that the observed changes in the photosynthesis response to temperature are not an artifact.

In this study (as in many others), the assumption was made that Rubisco kinetic parameters as determined in tobacco (i.e. following Bernacchi et al., 2002) adequately represent all PFTs. Recent studies have found notable differences in Rubisco kinetic parameters across plant types and species (Galmés, Hermida-Carrera, Laanisto, & Niinemets, 2016; Walker et al., 2013), and differences in Rubisco properties across plant types and climate conditions, as outlined in Galmés et al. (2016), should be included in future LSMs to better represent the temperature response of photosynthesis across the globe. However, so far no studies have determined Rubisco kinetic parameters on a $C_c$-basis across PFTs, which could be used in LSMs where $g_m$ is included explicitly. For use in models, it is essential that $C_c$-based Rubisco kinetic parameters, $g_m$, as well as their temperature responses, are measured on the same set of leaves (as in Bernacchi et al., 2002), in order to ensure consistency across photosynthetic parameters.

## 4.2 | Implications for water and carbon fluxes at ecosystem level

The adjustments to the photosynthesis model cause modest changes to the $CO_2$ sensitivity of $A_{n,canopy}$ and $G_c$. However, the responses depend on the type of $g_m$ model that is implemented. In the *Exp* version (no light and $C_i$ response), the sensitivity of $A_{n,canopy}$ and $G_c$ to $CO_2$ depends both on the magnitude of $g_m$ and the climatic conditions, foremost temperature. Strongest effects were found in cold ecosystems with a low $g_m$ (FI-Hyy), but this response does not hold across all climate types, and the tropical site GF-Guy showed the reverse response and a decreasing responsiveness to $eCO_2$.

The *ExpC* version ($C_i$ response) does not differ markedly from the *Exp* version described above for any of the ecosystems investigated here. This indicates that the parameter adjustment is capable of completely offsetting the $g_m$ response to $C_i$ by a concomitant increase in $J_{max25,Cc}$. This is an important implication for models as our results indicate that a potential response of $g_m$ to $C_i$ is not expected

to have an impact on the simulated response of carbon and water fluxes to $eCO_2$ in LSMs.

Contrarily, the *ExpL* version (light response) leads to a stronger $CO_2$ responsiveness of $A_{n,canopy}$ in all ecosystem types. This effect can best be demonstrated with leaf level simulations under low light conditions, where the $CO_2$ responsiveness of $A_{n,canopy}$ is higher in the *ExpL* compared to the *Imp* model, so long as $C_i$ is not saturating (Figure S7). This effect is amplified at the ecosystem level, where a certain fraction of the canopy operates in sub-saturating light conditions regardless of the amount of incident radiation. This potential light response of $g_m$ thus significantly increases the $CO_2$ sensitivity of all C3 ecosystems investigated here and amplifies the strong positive changes in photosynthetic responsiveness to $CO_2$ in cold climates, or compensates for the negative response in warmer climates.

The explicit representation of $g_m$ did not change simulations of $iWUE_{,canopy}$ ($A_{n,canopy}/G_c$), which increased at the same rate as in the implicit model version regardless of the $g_m$ model employed. This behavior is a consequence of the implemented stomatal conductance model (Medlyn et al., 2011), which is based on the strong coupling between $A_n$ and $g_s$, that causes the $C_i/C_a$ ratio to stay constant regardless of the atmospheric $CO_2$ concentration. Since most LSMs employ similar $g_s$ models as the one used here (see e.g. Sato, To, Takahashi, & Katul, 2015 for an overview), our results are in that respect likely representative for most LSMs.

Our results do not indicate changes to simulations of C4 photosynthesis when $g_m$ is considered explicitly. This is because the explicit consideration of $g_m$ was compensated by an increase in the PEP-carboxylation rate ($V_{pmax25}$) in the course of the parameter adjustment. While we acknowledge that we lack sufficient data to confidently parameterize the C4 photosynthesis model employed here (von Caemmerer & Furbank, 1999) at the global scale, we argue that, from a modeling point of view, results would be similar if the simpler and more widely used model by Collatz, Ribas-Carbo, and Berry (1992) (as described in e.g. Bonan et al., 2011) was used, in which case the consideration of $g_m$ would affect the slope of the initial $CO_2$ response curve in a similar manner as it affected $V_{pmax25}$ in the model of von Caemmerer and Furbank (1999) (see Figure S5).

## 4.3 | Global implications

Global simulations under anticipated future climate suggest clear and regionally contrasting effects of $g_m$ on GPP and transpiration. The differences between the $g_m$-implicit and $g_m$-explicit simulations depend on the projected climate, and on the PFT distribution through vegetation-type differences in the magnitude of $g_m$. The fact that plant groups with a low $g_m$ showed stronger responses to $eCO_2$ than those with a high $g_m$ under the same climate generally supports an earlier hypothesis that evergreen species are more likely to have a competitive advantage over other plant types in a high $CO_2$ world (Niinemets et al., 2011). However, our analysis suggests that this hypothesis does not hold in the tropics, where a low $g_m$ led to a decrease in the photosynthetic $CO_2$ responsiveness (Figures 5b and 6). However, the actual relevance of $g_m$ in present and future vegetation dynamics must still be investigated using experimental and modeling approaches.

The replacement of the $g_m$-implicit with a $g_m$-explicit model caused significant changes to simulations of GPP, ranging from 2.3 Pg C $yr^{-1}$ in the *Exp* model and the RCP4.5 scenario to 6.6 Pg C $yr^{-1}$ in the *ExpCL* model and the RCP8.5 scenario (Figure S11). About two thirds of this increase were caused by regions north of >30°N, where it mostly occurred in regions covered by boreal forests. Changes of this magnitude are likely large enough to significantly affect the amplitude of atmospheric $CO_2$ in the high latitudes, hence $g_m$, which is so far neglected in this context (Forkel et al., 2016; Zeng et al., 2014), should be considered as an additional explanatory factor.

Although our results are broadly consistent with those of Sun, Gu, Dickinson, Norby et al. (2014), our estimates of the GPP response to $CO_2$ are more moderate. Compared to the 16% increase in the cumulative GPP found by Sun, Gu, Dickinson, Norby et al. (2014), our results (calculated from Figure S13 using Equation (2) in Sun, Gu, Dickinson, Norby et al., 2014) suggest smaller changes in the order of 6% in the *Exp* model version and the RCP8.5 scenario (but similar values of 15% in the *ExpCL* scenario). However, these numbers may not be directly comparable due to different simulation periods. With respect to the latitudinal patterns of the $g_m$ effects, our results agree with those by Sun, Gu, Dickinson, Norby et al. (2014), as in both cases, the weakest and strongest effects were found in the tropics and the northern latitudes, respectively. Our simulations (Figure S12) further suggest clear differences in ET between the two model versions, which may have impacts on other physical land surface properties, such as land surface temperature, soil moisture, or sensible heat fluxes.

## 4.4 | Future model developments and research needs

Our results emphasize that the absolute value of $g_m$ is important for the adjustment of photosynthetic parameters and the associated effects on simulations of photosynthesis. The magnitude of $g_m$ is relatively robust for well-sampled PFTs, and similar to the results of earlier data compilations (Flexas et al., 2008), but more measurements are needed for tropical species, deciduous needle-leaf species, and C4 plants. The parameterization of these plant types is important for large-scale simulations, but their maximum $g_m$ values can at the moment not be confidently parameterized due to a lack of data. In addition, other plant groups such as ferns should be investigated in future LSMs. These plant groups are characterized by a low $g_m$ (Carriquí et al., 2015; Tosens et al., 2016), thus their consideration may have important effects on simulated water and carbon fluxes in models that explicitly simulate $g_m$.

It is clearly desirable to bring empirical formulations of $g_m$ as used here and in previous studies (Suits et al., 2005; Sun, Gu, Dickinson, Norby et al., 2014) to a more process-based representation. While

existing leaf-level models of $g_m$ (Tholen & Zhu, 2011; Tomás et al., 2013) are likely too complex to be parameterized at large scales, global models of $g_m$ could be readily improved by relating key model parameters (e.g. $g_{m,max25}$) to both anatomical (e.g. cell wall thickness, mesophyll porosity) (Peguero-Pina et al., 2017; Tomás et al., 2013), and biochemical plant traits (e.g. leaf nitrogen content) (von Caemmerer & Evans, 1991; Xue, Ko, Werner, & Tenhunen, 2017; Yamori, Nagai, & Makino, 2011) within a parsimonious model framework that can be applied across plant types.

Currently, one factor hampering future model development is the poor process understanding of $g_m$, which is associated with the fact that measurements of $g_m$ are challenging (Pons et al., 2009). It is particularly critical that the role of environmental factors such as $C_i$ and light is unresolved. Here, we tested the potential effects of these two drivers on large-scale simulations of carbon and water fluxes. We found that a potential $C_i$ response does not change model predictions, as its effects would be offset by the adjustment of $V_{cmax25}$ and $J_{max25}$ from their apparent to true values. A potential light response of $g_m$, however, would be amplified at canopy level and lead to a significantly higher responsiveness of $A_n$ to rising atmospheric $CO_2$ concentrations. Extrapolated to the global scale, such a leaf-level response would significantly increase global carbon uptake and water loss. It is thus highly relevant that potential measurement artifacts are ruled out (Gu & Sun, 2014), and that the recently put forward hypothesis of an apparent light response (Théroux-Rancourt & Gilbert, 2017) is investigated further, as its existence would mean that the light response of $g_m$ as observed at the leaf level should not be implemented in models.

## ACKNOWLEDGEMENTS

We thank Dr. Carl Bernacchi for helpful discussions on the parameter adjustment. SZ was supported by the European Research Council (ERC) under the European Union's Horizon 2020 research and innovation program (grant agreement no. 647204; QUINCY). MDK acknowledges support from the Australian Research Council Centre of Excellence for Climate Extremes (CE170100023).

## ORCID

*Jürgen Knauer* https://orcid.org/0000-0002-4947-7067
*Martin G. De Kauwe* https://orcid.org/0000-0002-3399-9098
*Belinda E. Medlyn* https://orcid.org/0000-0001-5728-9827

## REFERENCES

Bahar, N. H., Hayes, L., Scafaro, A. P., Atkin, O. K., & Evans, J. R. (2018). Mesophyll conductance does not contribute to greater photosynthetic rate per unit nitrogen in temperate compared with tropical evergreen wet-forest tree leaves. *New Phytologist*, *218*, 492–505. https://doi.org/10.1111/nph.15031

Barbour, M. M., Evans, J. R., Simonin, K. A., & Caemmerer, S. (2016). Online $CO_2$ and $H_2O$ oxygen isotope fractionation allows estimation of mesophyll conductance in C4 plants, and reveals that mesophyll conductance decreases as leaves age in both C4 and C3 plants. *New Phytologist*, *210*, 875–889.

Bellouin, N., Collins, W. J., Culverwell, I. D., Halloran, P. R., Hardiman, S. C., Hinton, T. J., … Wiltshire, A. (2011). The HadGEM2 family of Met Office Unified Model climate configurations. *Geoscientific Model Development*, *4*, 723–757. https://doi.org/10.5194/gmd-4-723-2011

Berbigier, P., Bonnefond, J.-M., & Mellmann, P. (2001). $CO_2$ and water vapour fluxes for 2 years above Euroflux forest site. *Agricultural and Forest Meteorology*, *108*, 183–197. https://doi.org/10.1016/S0168-1923(01)00240-4

Bernacchi, C. J., Portis, A. R., Nakano, H., von Caemmerer, S., & Long, S. P. (2002). Temperature response of mesophyll conductance. Implications for the determination of Rubisco enzyme kinetics and for limitations to photosynthesis in vivo. *Plant Physiology*, *130*, 1992–1998. https://doi.org/10.1104/pp.008250

Bernacchi, C., Singsaas, E., Pimentel, C., Portis, A. Jr, & Long, S. (2001). Improved temperature response functions for models of Rubisco-limited photosynthesis. *Plant, Cell & Environment*, *24*, 253–259. https://doi.org/10.1111/j.1365-3040.2001.00668.x

Bonal, D., Bosc, A., Ponton, S., Goret, J.-Y., Burban, B., Gross, P., … Granier, A. (2008). Impact of severe dry season on net ecosystem exchange in the Neotropical rainforest of French Guiana. *Global Change Biology*, *14*, 1917–1933. https://doi.org/10.1111/j.1365-2486.2008.01610.x

Bonan, G. B., Lawrence, P. J., Oleson, K. W., Levis, S., Jung, M., Reichstein, M., … Swenson, S. C. (2011). Improving canopy processes in the Community Land Model version 4 (CLM4) using global flux fields empirically inferred from FLUXNET data. *Journal of Geophysical Research, Biogeosciences*, 116. https://doi.org/10.1029/2010JG001593

Booth, B. B. B., Jones, C. D., Collins, M., Totterdell, I. J., Cox, P. M., Sitch, S., … Lloyd, J. (2012). High sensitivity of future global warming to land carbon cycle processes. *Environmental Research Letters*, *7*, 024002. https://doi.org/10.1088/1748-9326/7/2/024002

Cai, Y.-F., Yang, Q.-Y., Li, S.-F., Wang, J.-H., & Huang, W. (2017). The water-water cycle is a major electron sink in *Camellia* species when $CO_2$ assimilation is restricted. *Journal of Photochemistry and Photobiology B: Biology*, *168*, 59–66. https://doi.org/10.1016/j.jphotobiol.2017.01.024

Cano, F., Sánchez-Gómez, D., Gascó, A., Rodríguez-Calcerrada, J., Gil, L., Warren, C., & Aranda, I. (2011). Light acclimation at the end of the growing season in two broadleaved oak species. *Photosynthetica*, *49*, 581–592. https://doi.org/10.1007/s11099-011-0066-3

Carriquí, M., Cabrera, H. M., Conesa, M. À., Coopman, R. E., Douthe, C., Gago, J., … Flexas, J. (2015). Diffusional limitations explain the lower photosynthetic capacity of ferns as compared with angiosperms in a common garden study. *Plant, Cell & Environment*, *38*, 448–460. https://doi.org/10.1111/pce.12402

Collatz, G. J., Ribas-Carbo, M., & Berry, J. (1992). Coupled photosynthesis-stomatal conductance model for leaves of C4 plants. *Functional Plant Biology*, *19*, 519–538. https://doi.org/10.1071/PP9920519

Delfine, S., Loreto, F., Pinelli, P., Tognetti, R., & Alvino, A. (2005). Isoprenoids content and photosynthetic limitations in rosemary and spearmint plants under water stress. *Agriculture, Ecosystems & Environment*, *106*, 243–252. https://doi.org/10.1016/j.agee.2004.10.012

Douthe, C., Dreyer, E., Brendel, O., & Warren, C. R. (2012). Is mesophyll conductance to $CO_2$ in leaves of three Eucalyptus species sensitive to short-term changes of irradiance under ambient as well as low $O_2$? *Functional Plant Biology*, *39*, 435–448.

Egea, G., González-Real, M. M., Baille, A., Nortes, P. A., & Diaz-Espejo, A. (2011). Disentangling the contributions of ontogeny and water stress to photosynthetic limitations in almond trees. *Plant, Cell & Environment*, *34*, 962–979.

Egea, G., Verhoef, A., & Vidale, P. L. (2011). Towards an improved and more flexible representation of water stress in coupled

photosynthesis-stomatal conductance models. *Agricultural and Forest Meteorology*, *151*, 1370–1384.

Ethier, G., & Livingston, N. (2004). On the need to incorporate sensitivity to $CO_2$ transfer conductance into the Farquhar-von Caemmerer-Berry leaf photosynthesis model. *Plant, Cell & Environment*, *27*, 137–153. https://doi.org/10.1111/j.1365-3040.2004.01140.x

Evans, J. R., Caemmerer, S., Setchell, B. A., & Hudson, G. S. (1994). The relationship between $CO_2$ transfer conductance and leaf anatomy in transgenic tobacco with a reduced content of Rubisco. *Functional Plant Biology*, *21*, 475–495. https://doi.org/10.1071/PP9940475

Evans, J. R., Kaldenhoff, R., Genty, B., & Terashima, I. (2009). Resistances along the $CO_2$ diffusion pathway inside leaves. *Journal of Experimental Botany*, *60*, 2235–2248. https://doi.org/10.1093/jxb/erp117

Evans, J. R., & von Caemmerer, S. (2013). Temperature response of carbon isotope discrimination and mesophyll conductance in tobacco. *Plant, Cell & Environment*, *36*, 745–756. https://doi.org/10.1111/j.1365-3040.2012.02591.x

Farquhar, G., von Caemmerer, S., & Berry, J. (1980). A biochemical model of photosynthetic $CO_2$ assimilation in leaves of C3 species. *Planta*, *149*, 78–90. https://doi.org/10.1007/BF00386231

Flexas, J., Díaz-Espejo, A., Conesa, M., Coopman R. E., Douthe C., Gago, J., … Niinemets, Ü. (2016). Mesophyll conductance to $CO_2$ and Rubisco as targets for improving intrinsic water use efficiency in C3 plants. *Plant, Cell & Environment*, *39*, 965–982.

Flexas, J., Diaz-Espejo, A., Galmés, J., Kaldenhoff, R., Medrano, H., & Ribas-Carbo, M. (2007). Rapid variations of mesophyll conductance in response to changes in $CO_2$ concentration around leaves. *Plant, Cell & Environment*, *30*, 1284–1298.

Flexas, J., Ribas-Carbó, M., Diaz-Espejo, A., Galmés, J., & Medrano, H. (2008). Mesophyll conductance to $CO_2$: Current knowledge and future prospects. *Plant, Cell & Environment*, *31*, 602–621.

Forkel, M., Carvalhais, N., Rodenbeck, C., Keeling, R., Heimann, M., Thonicke, K., … Reichstein, M. (2016). Enhanced seasonal $CO_2$ exchange caused by amplified plant productivity in northern ecosystems. *Science*, *351*, 696–699. https://doi.org/10.1126/science.aac4971

Frieler, K., Lange, S., Piontek, F., Reyer, C. P. O., Schewe, J., Warszawski, L., … Yamagata, Y. (2017). Assessing the impacts of 1.5 °C global warming-simulation protocol of the Inter-Sectoral Impact Model Intercomparison Project (ISIMIP2b). *Geoscientific Model Development*, *10*, 4321–4345. https://doi.org/10.5194/gmd-10-4321-2017

Galmés, J., Abadía, A., Medrano, H., & Flexas, J. (2007). Photosynthesis and photoprotection responses to water stress in the wild-extinct plant *Lysimachia minoricensis*. *Environmental and Experimental Botany*, *60*, 308–317.

Galmés, J., Hermida-Carrera, C., Laanisto, L., & Niinemets, Ü. (2016). A compendium of temperature responses of Rubisco kinetic traits: Variability among and within photosynthetic groups and impacts on photosynthesis modeling. *Journal of Experimental Botany*, *67*, 5067–5091. https://doi.org/10.1093/jxb/erw267

Galmés, J., Medrano, H., & Flexas, J. (2007). Photosynthetic limitations in response to water stress and recovery in Mediterranean plants with different growth forms. *New Phytologist*, *175*, 81–93.

Giorgetta, M. A., Jungclaus, J., Reick, C. H., Legutke, S., Bader, J., Böttinger, M., … Stevens, B. (2013). Climate and carbon cycle changes from 1850 to 2100 in MPI-ESM simulations for the Coupled Model Intercomparison Project phase 5. *Journal of Advances in Modeling Earth Systems*, *5*, 572–597. https://doi.org/10.1002/jame.20038

Goudriaan, J. (1977). *Crop micrometeorology: A simulation study*. Pudoc, Wageningen, Netherlands: Center for Agricultural Publishing and Documentation.

Gu, L., Pallardy, S. G., Tu, K., Law, B. E., & Wullschleger, S. D. (2010). Reliable estimation of biochemical parameters from C3 leaf photosynthesis-intercellular carbon dioxide response curves. *Plant, Cell & Environment*, *33*, 1852–1874. https://doi.org/10.1111/j.1365-3040.2010.02192.x

Gu, L., & Sun, Y. (2014). Artefactual responses of mesophyll conductance to $CO_2$ and irradiance estimated with the variable J and online isotope discrimination methods. *Plant, Cell & Environment*, *37*, 1231–1249.

Han, Q., Iio, A., Naramoto, M., & Kakubari, Y. (2010). Response of internal conductance to soil drought in sun and shade leaves of adult *Fagus crenata*. *Acta Silvatica & Lignaria Hungarica*, *6*, 123–133.

Hanba, Y., Kogami, H., & Terashima, I. (2002). The effect of growth irradiance on leaf anatomy and photosynthesis in *Acer* species differing in light demand. *Plant, Cell & Environment*, *25*, 1021–1030. https://doi.org/10.1046/j.1365-3040.2002.00881.x

Hassiotou, F., Ludwig, M., Renton, M., Veneklaas, E. J., & Evans, J. R. (2009). Influence of leaf dry mass per area, $CO_2$, and irradiance on mesophyll conductance in sclerophylls. *Journal of Experimental Botany*, *60*, 2303–2314. https://doi.org/10.1093/jxb/erp021

Hempel, S., Frieler, K., Warszawski, L., Schewe, J., & Piontek, F. (2013). A trend-preserving bias correction-the ISI-MIP approach. *Earth System Dynamics*, *4*, 219–236.

Johnson, F. H., Eyring, H., & Williams, R. (1942). The nature of enzyme inhibitions in bacterial luminescence: Sulfanilamide, urethane, temperature and pressure. *Journal of Cellular Physiology*, *20*, 247–268. https://doi.org/10.1002/jcp.1030200302

Kala, J., De Kauwe, M. G., Pitman, A. J., Medlyn, B. E., Wang, Y.-P., Lorenz, R., & Perkins-Kirkpatrick, S. E. (2016). Impact of the representation of stomatal conductance on model projections of heatwave intensity. *Scientific Reports*, *6*.

Kattge, J., Díaz, S., Lavorel, S., Prentice, I. C., Leadley, P., Bönisch, G., … Wirth, C. (2011). TRY - a global database of plant traits. *Global Change Biology*, *17*, 2905–2935. https://doi.org/10.1111/j.1365-2486.2011.02451.x

Kattge, J., Knorr, W., Raddatz, T., & Wirth, C. (2009). Quantifying photosynthetic capacity and its relationship to leaf nitrogen content for global-scale terrestrial biosphere models. *Global Change Biology*, *15*, 976–991. https://doi.org/10.1111/j.1365-2486.2008.01744.x

Kirschbaum, M. (1994). The sensitivity of C3 photosynthesis to increasing $CO_2$ concentration: A theoretical analysis of its dependence on temperature and background $CO_2$ concentration. *Plant, Cell & Environment*, *17*, 747–754. https://doi.org/10.1111/j.1365-3040.1994.tb00167.x

Kitao, M., Yazaki, K., Kitaoka, S., Fukatsu, E., Tobita, H., Komatsu, M., … Koike, T. (2015). Mesophyll conductance in leaves of Japanese white birch (*Betula platyphylla* var. *japonica*) seedlings grown under elevated $CO_2$ concentration and low N availability. *Physiologia Plantarum*, *155*, 435–445. https://doi.org/10.1111/ppl.12335

Knauer, J., Werner, C., & Zaehle, S. (2015). Evaluating stomatal models and their atmospheric drought response in a land surface scheme: A multibiome analysis. *Journal of Geophysical Research: Biogeosciences*, *120*, 1894–1911. https://doi.org/10.1002/2015JG003114

Knauer, J., Zaehle, S., Reichstein, M., Medlyn, B. E., Forkel, M., Hagemann, S., & Werner, C. (2017). The response of ecosystem water-use efficiency to rising atmospheric $CO_2$ concentrations: Sensitivity and large-scale biogeochemical implications. *New Phytologist*, *213*, 1654–1666.

Kolbe, A. R., & Cousins, A. B. (2018). Mesophyll conductance in *Zea mays* responds transiently to $CO_2$ availability: implications for transpiration efficiency in $C_4$ crops. *New Phytologist*, *217*, 1463–1474.

Kutsch, W. l., Aubinet, M., Buchmann, N., Smith, P., Osborne, B., Eugster, W., … Ziegler, W. (2010). The net biome production of full crop rotations in Europe. *Agriculture, Ecosystems and Environment*, *139*, 336–345. https://doi.org/10.1016/j.agee.2010.07.016

Lin, Y.-S., Medlyn, B. E., Duursma, R. A., Prentice, I. C., Wang, H., Baig, S., … Wingate, L. (2015). Optimal stomatal behaviour around the world. *Nature Climate Change*, *5*, 459–464. https://doi.org/10.1038/nclimate2550

Loucos, K. E., Simonin, K. A., & Barbour, M. M. (2017). Leaf hydraulic conductance and mesophyll conductance are not closely related within

a single species. *Plant, Cell & Environment*, *40*, 203–215. https://doi.org/10.1111/pce.12865

Medlyn, B. E., Duursma, R. A., Eamus, D., Ellsworth, D. S., Prentice, I. C., Barton, C. V. M., … Wingate, L. (2011). Reconciling the optimal and empirical approaches to modelling stomatal conductance. *Global Change Biology*, *17*, 2134–2144. https://doi.org/10.1111/j.1365-2486.2010.02375.x

Misson, L., Limousin, J., Rodriguez, R., & Letts, M. G. (2010). Leaf physiological responses to extreme droughts in Mediterranean *Quercus ilex* forest. *Plant, Cell & Environment*, *33*, 1898–1910. https://doi.org/10.1111/j.1365-3040.2010.02193.x

Miyazawa, S.-I., Yoshimura, S., Shinzaki, Y., Maeshima, M., & Miyake, C. (2008). Deactivation of aquaporins decreases internal conductance to $CO_2$ diffusion in tobacco leaves grown under long-term drought. *Functional Plant Biology*, *35*, 553–564. https://doi.org/10.1071/FP08117

Mizokami, Y., Noguchi, K., Kojima, M., Sakakibara, H., & Terashima, I. (2018). Effects of instantaneous and growth $CO_2$ levels and abscisic acid on stomatal and mesophyll conductances. *Plant, Cell & Environment*, 1–13. https://doi.org/10.1111/pce.13484

Montpied, P., Granier, A., & Dreyer, E. (2009). Seasonal time-course of gradients of photosynthetic capacity and mesophyll conductance to $CO_2$ across a beech (*Fagus sylvatica* L.) canopy. *Journal of Experimental Botany*, *60*, 2407–2418. https://doi.org/10.1093/jxb/erp093

Niinemets, Ü., Díaz-Espejo, A., Flexas, J., Galmés, J., & Warren, C. R. (2009). Importance of mesophyll diffusion conductance in estimation of plant photosynthesis in the field. *Journal of Experimental Botany*, *60*, 2271–2282. https://doi.org/10.1093/jxb/erp063

Niinemets, Ü., Flexas, J., & Peñuelas, J. (2011). Evergreens favored by higher responsiveness to increased $CO_2$. *Trends in Ecology & Evolution*, *26*, 136–142. https://doi.org/10.1016/j.tree.2010.12.012

Niinemets, Ü., Cescatti, A., Rodeghiero, M., & Tosens, T. (2006). Complex adjustments of photosynthetic potentials and internal diffusion conductance to current and previous light availabilities and leaf age in Mediterranean evergreen species *Quercus ilex*. *Plant, Cell & Environment*, *29*, 1159–1178. https://doi.org/10.1111/j.1365-3040.2006.01499.x

Peguero-Pina, J. J., Sisó, S., Flexas, J., Galmés, J., García-Nogales, A., Niinemets, Ü., … Gil-Pelegrín, E. (2017). Cell-level anatomical characteristics explain high mesophyll conductance and photosynthetic capacity in sclerophyllous Mediterranean oaks. *New Phytologist*, *214*, 585–596. https://doi.org/10.1111/nph.14406

Perez-Martin, A., Michelazzo, C., Torres-Ruiz, J. M., Flexas, J., Fernández, J. E., Sebastiani, L., & Diaz-Espejo, A. (2014). Regulation of photosynthesis and stomatal and mesophyll conductance under water stress and recovery in olive trees: Correlation with gene expression of carbonic anhydrase and aquaporins. *Journal of Experimental Botany*, *65*, 3143–3156. https://doi.org/10.1093/jxb/eru160

Piel, C., Frak, E., Le Roux, X., & Genty, B. (2002). Effect of local irradiance on $CO_2$ transfer conductance of mesophyll in walnut. *Journal of Experimental Botany*, *53*, 2423–2430. https://doi.org/10.1093/jxb/erf095

Pongratz, J., Reick, C., Raddatz, T., & Claussen, M. (2007). Reconstruction of global land use and land cover AD 800 to 1992. https://doi.org/10.1594/WDCC/RECON_LAND_COVER_800-1992

Pons, T. L., Flexas, J., Von Caemmerer, S., Evans, J. R., Genty, B., Ribas-Carbo, M., & Brugnoli, E. (2009). Estimating mesophyll conductance to $CO_2$: Methodology, potential errors, and recommendations. *Journal of Experimental Botany*, *60*, 2217–2234. https://doi.org/10.1093/jxb/erp081

Rambal, S., Ourcival, J.-M., Joffre, R., Mouillot, F., Nouvellon, Y., Reichstein, M., & Rocheteau, A. (2003). Drought controls over conductance and assimilation of a Mediterranean evergreen ecosystem: Scaling from leaf to canopy. *Global Change Biology*, *9*, 1813–1824. https://doi.org/10.1111/j.1365-2486.2003.00687.x

Reick, C., Raddatz, T., Brovkin, V., & Gayler, V. (2013). Representation of natural and anthropogenic land cover change in MPI-ESM. *Journal of Advances in Modeling Earth Systems*, *5*, 459–482. https://doi.org/10.1002/jame.20022

Rogers, A., Medlyn, B. E., Dukes, J. S., Bonan, G., von Caemmerer, S., Dietze, M. C., … Zaehle, S. (2017). A roadmap for improving the representation of photosynthesis in Earth system models. *New Phytologist*, *213*, 22–42. https://doi.org/10.1111/nph.14283

Sato, H., To, K., Takahashi, A., & Katul, G. G. (2015). Effects of different representations of stomatal conductance response to humidity across the African continent under warmer $CO_2$-enriched climate conditions. *Journal of Geophysical Research: Biogeosciences*, *120*, 979–988.

Scafaro, A. P., Von Caemmerer, S., Evans, J. R., & Atwell, B. J. (2011). Temperature response of mesophyll conductance in cultivated and wild *Oryza* species with contrasting mesophyll cell wall thickness. *Plant, Cell & Environment*, *34*, 1999–2008. https://doi.org/10.1111/j.1365-3040.2011.02398.x

Schulz, J.-P., Dümenil, L., & Polcher, J. (2001). On the land surface-atmosphere coupling and its impact in a single-column atmospheric model. *Journal of Applied Meteorology*, *40*, 642–663. https://doi.org/10.1175/1520-0450(2001)040<0642:OTLSAC>2.0.CO;2

Singsaas, E., Ort, D., & Delucia, E. (2003). Elevated $CO_2$ effects on mesophyll conductance and its consequences for interpreting photosynthetic physiology. *Plant, Cell & Environment*, *27*, 41–50. https://doi.org/10.1046/j.0016-8025.2003.01123.x

Suits, N. S., Denning, A. S., Berry, J., Still, C., Kaduk, J., Miller, J., & Baker, I. (2005). Simulation of carbon isotope discrimination of the terrestrial biosphere. *Global Biogeochemical Cycles*, *19*, https://doi.org/10.1029/2003GB002141

Sun, Y., Gu, L., Dickinson, R. E., Norby, R. J. Pallardy, S. G., & Hoffman, F. M. (2014) Impact of mesophyll diffusion on estimated global land $CO_2$ fertilization. *Proceedings of the National Academy of Sciences*. 201418075.

Sun, Y., Gu, L., Dickinson, R. E., Pallardy, S. G., Baker, J., Cao, Y., & Winter, K. (2014). Asymmetrical effects of mesophyll conductance on fundamental photosynthetic parameters and their relationships estimated from leaf gas exchange measurements. *Plant, Cell & Environment*, *37*, 978–994.

Tazoe, Y., Von Caemmerer, S., Badger, M. R., & Evans, J. R. (2009). Light and $CO_2$ do not affect the mesophyll conductance to $CO_2$ diffusion in wheat leaves. *Journal of Experimental Botany*, *60*, 2291–2301. https://doi.org/10.1093/jxb/erp035

Théroux-Rancourt, G., & Gilbert, M. E. (2017). The light response of mesophyll conductance is controlled by structure across leaf profiles. *Plant, Cell & Environment*, *40*, 726–740. https://doi.org/10.1111/pce.12890

Tholen, D., & Zhu, X.-G. (2011). The mechanistic basis of internal conductance: A theoretical analysis of mesophyll cell photosynthesis and $CO_2$ diffusion. *Plant Physiology*, *156*, 90–105. https://doi.org/10.1104/pp.111.172346

Tomás, M., Flexas, J., Copolovici, L., Galmés, J., Hallik, L., Medrano, H., … Niinemets, Ü. (2013). Importance of leaf anatomy in determining mesophyll diffusion conductance to $CO_2$ across species: Quantitative limitations and scaling up by models. *Journal of Experimental Botany*, *64*, 2269–2281. https://doi.org/10.1093/jxb/ert086

Tosens, T., Nishida, K., Gago, J., Coopman, R. E., Cabrera, H. M., Carriquí, M., … Flexas, J. (2016). The photosynthetic capacity in 35 ferns and fern allies: Mesophyll $CO_2$ diffusion as a key trait. *New Phytologist*, *209*, 1576–1590. https://doi.org/10.1111/nph.13719

Ubierna, N., Gandin, A., Boyd, R. A., & Cousins, A. B. (2017). Temperature response of mesophyll conductance in three $C_4$ species calculated with two methods: $^{18}O$ discrimination and *in vitro* $V_{pmax}$. *New Phytologist*, *214*, 66–80. https://doi.org/10.1111/nph.14359

Urbanski, S., Barford, C., Wofsy, S., Kucharik, C., Pyle, E., Budney, J., … Munger, J. W. (2007). Factors controlling $CO_2$ exchange on timescales from hourly to decadal at Harvard Forest. *Journal of Geophysical Research: Biogeosciences*, *112*, G02020.

Varone, L., Ribas-Carbo, M., Cardona, C., Gallé, A., Medrano, H., Gratani, L., & Flexas, J. (2012). Stomatal and non-stomatal limitations to photosynthesis in seedlings and saplings of Mediterranean species pre-conditioned and aged in nurseries: Different response to water stress. *Environmental and Experimental Botany*, *75*, 235–247. https://doi.org/10.1016/j.envexpbot.2011.07.007

Verma, S. B., Dobermann, A., Cassman, K. G., Walters, D. T., Knops, J. M., Arkebauer, T. J., … Walter-Shea, E. A. (2005). Annual carbon dioxide exchange in irrigated and rainfed maize-based agroecosystems. *Agricultural and Forest Meteorology*, *131*, 77–96. https://doi.org/10.1016/j.agrformet.2005.05.003

Vesala, T., Suni, T., Rannik, Ü., Keronen, P., Markkanen, T., Sevanto, S., … Hari, P. (2005). Effect of thinning on surface fluxes in a boreal forest. *Global Biogeochemical Cycles*, *19*. https://doi.org/10.1029/2004GB002316

von Caemmerer, S., & Evans, J. R. (1991). Determination of the average partial pressure of $CO_2$ in chloroplasts from leaves of several C3 plants. *Functional Plant Biology*, *18*, 287–305. https://doi.org/10.1071/PP9910287

von Caemmerer, S., & Evans, J. R. (2015). Temperature responses of mesophyll conductance differ greatly between species. *Plant, Cell & Environment*, *38*, 629–637. https://doi.org/10.1111/pce.12449

von Caemmerer, S., & Furbank, R. T. (1999). Modeling C4 photosynthesis. In R. F. Sage, & R. K. Monson (Eds.), *C4 plant biology* (pp. 173–211). Canada, ON: Academic Press Toronto.

Walker, B., Ariza, L. S., Kaines, S., Badger, M. R., & Cousins, A. B. (2013). Temperature response of *in vivo* Rubisco kinetics and mesophyll conductance in *Arabidopsis thaliana*: Comparisons to *Nicotiana tabacum*. *Plant, Cell & Environment*, *36*, 2108–2119.

Wang, Y. P. (2003). A comparison of three different canopy radiation models commonly used in plant modelling. *Functional Plant Biology*, *30*, 143–152. https://doi.org/10.1071/FP02117

Warren, C. R. (2008). Stand aside stomata, another actor deserves centre stage: The forgotten role of the internal conductance to $CO_2$ transfer. *Journal of Experimental Botany*, *59*, 1475–1487. https://doi.org/10.1093/jxb/erm245

Warren, C., Löw, M., Matyssek, R., & Tausz, M. (2007). Internal conductance to $CO_2$ transfer of adult *Fagus sylvatica*: Variation between sun and shade leaves and due to free-air ozone fumigation. *Environmental and Experimental Botany*, *59*, 130–138. https://doi.org/10.1016/j.envexpbot.2005.11.004

Wohlfahrt, G., Hammerle, A., Haslwanter, A., Bahn, M., Tappeiner, U., & Cernusca, A. (2008). Seasonal and inter-annual variability of the net ecosystem $CO_2$ exchange of a temperate mountain grassland: Effects of weather and management. *Journal of Geophysical Research-Atmospheres*, *113*.

Wong, S., Cowan, I., & Farquhar, G. (1979). Stomatal conductance correlates with photosynthetic capacity. *Nature*, *282*, 424–426. https://doi.org/10.1038/282424a0

Xiong, D., Liu, X., Liu, L., Douthe, C., Li, Y., Peng, S., & Huang, J. (2015). Rapid responses of mesophyll conductance to changes of $CO_2$ concentration, temperature and irradiance are affected by N supplements in rice. *Plant, Cell & Environment*, *38*, 2541–2550.

Xue, W., Ko, J., Werner, C., & Tenhunen, J. (2017). A spatially hierarchical integration of close-range remote sensing, leaf structure and physiology assists in diagnosing spatiotemporal dimensions of field-scale ecosystem photosynthetic productivity. *Agricultural and Forest Meteorology*, *247*, 503–519. https://doi.org/10.1016/j.agrformet.2017.08.038

Yamori, W., Evans, J. R., & Von Caemmerer, S. (2010). Effects of growth and measurement light intensities on temperature dependence of $CO_2$ assimilation rate in tobacco leaves. *Plant, Cell & Environment*, *33*, 332–343.

Yamori, W., Nagai, T., & Makino, A. (2011). The rate-limiting step for $CO_2$ assimilation at different temperatures is influenced by the leaf nitrogen content in several C3 crop species. *Plant, Cell & Environment*, *34*, 764–777. https://doi.org/10.1111/j.1365-3040.2011.02280.x

Yin, X., Struik, P. C., Romero, P., Harbinson, J., Evers, J. B., Van Der Putten, P. E., & Vos, J. (2009). Using combined measurements of gas exchange and chlorophyll fluorescence to estimate parameters of a biochemical C3 photosynthesis model: A critical appraisal and a new integrated approach applied to leaves in a wheat (*Triticum aestivum*) canopy. *Plant, Cell & Environment*, *32*, 448–464.

Zaehle, S., & Friend, A. (2010). Carbon and nitrogen cycle dynamics in the O-CN land surface model: 1. Model description, site-scale evaluation, and sensitivity to parameter estimates. *Global Biogeochemical, Cycles*, 24.

Zeng, N., Zhao, F., Collatz, G. J., Kalnay, E., Salawitch, R. J., West, T. O., & Guanter, L. (2014). Agricultural Green Revolution as a driver of increasing atmospheric $CO_2$ seasonal amplitude. *Nature*, *515*, 394–397. https://doi.org/10.1038/nature13893

Zhang, S.-B., & Yin, L.-X. (2012). Plasticity in photosynthesis and functional leaf traits of *Meconopsis horridula* var. *racemosa* in response to growth irradiance. *Botanical Studies*, *53*, 335–343.

## SUPPORTING INFORMATION

Additional supporting information may be found online in the Supporting Information section at the end of the article.

**How to cite this article:** Knauer J, Zaehle S, De Kauwe MG, et al. Effects of mesophyll conductance on vegetation responses to elevated $CO_2$ concentrations in a land surface model. *Glob Change Biol.* 2019;25:1820–1838. https://doi.org/10.1111/gcb.14604